



This is a repository copy of *A thermodynamic model for C-(N-)A-S-H gel: CNASH_ss. Derivation and validation.*

White Rose Research Online URL for this paper:
<http://eprints.whiterose.ac.uk/97067/>

Version: Accepted Version

Article:

Myers, R.J., Bernal, S.A. and Provis, J.L. orcid.org/0000-0003-3372-8922 (2014) A thermodynamic model for C-(N-)A-S-H gel: CNASH_ss. Derivation and validation. Cement and Concrete Research, 66. pp. 27-47. ISSN 0008-8846

<https://doi.org/10.1016/j.cemconres.2014.07.005>

Article available under the terms of the CC-BY-NC-ND licence
(<https://creativecommons.org/licenses/by-nc-nd/4.0/>)

Reuse

This article is distributed under the terms of the Creative Commons Attribution-NonCommercial-NoDerivs (CC BY-NC-ND) licence. This licence only allows you to download this work and share it with others as long as you credit the authors, but you can't change the article in any way or use it commercially. More information and the full terms of the licence here: <https://creativecommons.org/licenses/>

Takedown

If you consider content in White Rose Research Online to be in breach of UK law, please notify us by emailing eprints@whiterose.ac.uk including the URL of the record and the reason for the withdrawal request.



eprints@whiterose.ac.uk
<https://eprints.whiterose.ac.uk/>

A thermodynamic model for C-(N-)A-S-H gel:

CNASH_{ss}. Derivation and validation

Rupert J. Myers, Susan A. Bernal, John L. Provis *

Department of Materials Science and Engineering, The University of Sheffield, Sir Robert
Hadfield Building, Mappin St, Sheffield S1 3JD, UK

* To whom correspondence should be addressed. Email j.provis@sheffield.ac.uk, phone
+44 114 222 5490, fax +44 114 222 5493

Abstract

The main reaction product in Ca-rich alkali-activated cements and hybrid Portland cement (PC)-based materials is an calcium (alkali) aluminosilicate hydrate (C-(N-)A-S-H) gel. Thermodynamic models without explicit definitions of structurally-incorporated Al species have been used in numerous past studies to describe this gel, but offer limited ability to simulate the chemistry of blended PC materials and alkali-activated cements. Here, a thermodynamic model for C-(N-)A-S-H gel is derived and parameterised to describe solubility data for the CaO-(Na₂O,Al₂O₃)-SiO₂-H₂O systems and alkali-activated slag (AAS) cements, and to chemical composition data for C-A-S-H gels. Simulated C-(N-)A-S-H gel densities and molar volumes are consistent with the corresponding values reported for AAS cements, meaning that the model can be used to describe chemical shrinkage in

24 these materials. Therefore, this model can provide insight into the chemistry of AAS cements at
25 advanced ages, which is important for understanding the long-term durability of these materials.

26

27

28 **Keywords**

29

30 *B. Calcium-Silicate-Hydrate (C-S-H); B. Thermodynamic Calculations; D. Alkali Activated Cement; D.*

31 *Blended Cement; E. Modelling.*

32

33

34 **Nomenclature**

35

a	Extent of substitution of trivalent cation R in bridging sites
\dot{a}	Ion size parameter in the extended Debye-Hückel equation (Å)
a', b', \dots, e'	Stoichiometric coefficients in the additivity method
A_γ	Temperature-dependent electrostatic parameter in the extended Debye-Hückel equation
BCI	Combined BT , CB and IC sites ($BCI = BT + CB + IC$)
b^{sc}	Neutron scattering length (m)
BT	Bridging tetrahedra
B_γ	Pressure-dependent electrostatic parameter in the extended Debye-Hückel equation
b_γ	Short-range interaction parameter in the extended Debye-Hückel equation, $\text{kg}\cdot\text{mol}^{-1}$
c	Charge of the charge-balancing interlayer cation
CB	Interlayer charge-balancing species for bridging tetrahedra
CL	Chain length of an end-member in the sublattice solid solution model
Cp^o	Absolute isobaric heat capacity at standard state ($\text{J}\cdot\text{mol}^{-1}\cdot\text{K}^{-1}$)
CU	Interstitial 'solid solution' $\text{Ca}(\text{OH})_2$
d_1, d_2	Coefficients for the CB sites
e_1, e_2	Coefficients for the IC sites
$\Delta_f G^o$	Standard Gibbs free energy of formation ($\text{J}\cdot\text{mol}^{-1}$)
G_m	Gibbs free energy of mixing ($\text{J}\cdot\text{mol}^{-1}$)
G_m^E	Excess Gibbs free energy of mixing ($\text{J}\cdot\text{mol}^{-1}$)
h	The amount of water per dreierketten unit in a tobermorite-like structure
$\Delta_f H^o$	Standard enthalpy of formation ($\text{J}\cdot\text{mol}^{-1}$)

i	Species of the sublattice solid solution model
I	Ionic strength of the aqueous electrolyte phase in the extended Debye-Hückel equation, mol·kg ⁻¹
I, II, III, IV, V, VI	Stoichiometric coefficients of the sublattice sites in the solid solution model
$i_1i_2i_3...i_s$	End-member of the sublattice solid solution model written in terms of the species substituted in sublattice sites 1, 2, 3,..., s
IC	Interlayer charge-balancing species for the TU sites
IW	Interlayer water
k	End-member of the sublattice solid solution model
K_{so}	Solubility product
l	Charge-balancing interlayer cation
MW	Molecular weight (g·mol ⁻¹)
N_A	Avogadro constant (6.022 x 10 ²³ mol ⁻¹)
n_s	Sublattice sites
R	Trivalent cation in tetrahedral coordination
R^*	Universal gas constant (8.3145 J·mol ⁻¹ ·K ⁻¹)
s	Index of sublattice site n
S^o	Absolute entropy at standard state (J·mol ⁻¹ ·K ⁻¹)
T	Temperature (K)
TU	Main chain site, CaSiO _{3.5} ⁻
u	Interlayer H ⁺ content per dreierketten unit for the TU sites
U	Term containing the Gibbs free energies for the reciprocal reactions (J·mol ⁻¹)
V^o	Standard molar volume (J·bar ⁻¹)
x_{jw}	Molar quantity of water in the extended Debye-Hückel equation, mol
X_w	Total molar amount of the aqueous phase in the extended Debye-Hückel equation, mol
y_i^{ns}	Site fraction of species i in the sublattice site n_s
z_j	Charge of aqueous species j
α_k	Activity of end-member k
γ_j	Activity coefficient of aqueous species j
Δ_{rcp}^oG	Standard Gibbs free energy of a reciprocal reaction between end-members of the sublattice solid solution model
ζ	Stoichiometric coefficient of the s^{th} sublattice site
λ_k	Fictive activity coefficient of end-member k
μ	Chemical potential (J·mol ⁻¹)
ν	Fraction of bridging site vacancies per dreierketten unit
ρ'	Density of an end-member of the sublattice solid solution model (g·m ⁻³)
ρ^{sc}	Neutron scattering length density (m ⁻²)
Φ^o	Standard thermodynamic property estimated by the additivity method
$\chi_k^{i,ns}$	Effective mole fraction of end-member k containing species i in sublattice site n_s

36

37

38

39 **1. Introduction**

40

41 A key factor governing the long-term performance of any cement or concrete is the stability of the
42 reaction products constituting the solid binder. Work in this area has historically been targeted at
43 understanding the chemistry of the primary reaction product in Portland cement (PC) materials,
44 which is a Ca-rich ($\text{Ca/Si} > 1.5$) calcium silicate hydrate (C-S-H)^a gel [1]. A substantial amount of this
45 research has been devoted to understanding the solubility of C-S-H gel [2-16], and development of
46 thermodynamic models for this phase has been ongoing over the past decades [15, 17-22]. The Kulik
47 and Kersten C-S-H thermodynamic model [17] has been applied extensively to successfully predict
48 hydrated PC solid phase assemblages and pore solution compositions as a function of the bulk solid
49 binder chemistry [23, 24]. The majority of published solubility data for C-S-H gel have been identified
50 to fall onto several distinct solubility curves [8, 16], indicating that an important and complex
51 structure-solubility relationship exists for this phase. More recently, a structurally-consistent C-S-H
52 thermodynamic model has been developed [25], which has further improved the utility of the
53 thermodynamic modelling approach in understanding the chemistry of PC materials.

54

55 Although the chemistry of hydrated neat PC materials is now relatively well established, many
56 modern cements are comprised of blends of PC with Al-containing supplementary cementitious
57 materials (SCMs), which react to form calcium aluminosilicate hydrate (C-A-S-H) gels with
58 significantly lower Ca content ($\text{Ca/Si} \leq 1.5$) [26, 27]. The level of Ca in the gel is reduced even further
59 in alkali-activated slag (AAS) cements, which are formed through the reaction between ground
60 granulated blast furnace slag (GBFS) and a highly alkaline solution (which are most often Na-based,
61 although the products of activation with alternative alkalis such as K are generally similar [28]). The
62 compositions of the C-A-S-H type gels formed in these cements (denoted C-(N)-A-S-H to reflect the

^a Cement chemistry shorthand notation is used throughout the text: A, Al_2O_3 ; C, CaO; S, SiO_2 ; H, H_2O ; and N, Na_2O .

63 increased alkali content in addition to the high levels of Al incorporated into this phase) vary
64 depending on the activation conditions, but are typically close to $\text{Ca/Si} = 1$ [29].

65

66 Previous thermodynamic studies of PC/SCM blended cements [26, 30] and AAS cements [31] have
67 utilised empirical descriptions of Al substitution in C-A-S-H and C-(N-)A-S-H gels (e.g. by attributing
68 amounts of Al to these gels to match experimentally measured Al/Si values of the solid binders in
69 the materials), or have neglected to account for the uptake of Al into these phases in the modelling
70 performed, because existing C-S-H thermodynamic model formulations do not contain explicit
71 definitions of Al [15, 17, 18, 21, 25]. The ability to formally account for the extent of Al incorporation
72 into these models is important because it offers scope to significantly improve the level of detail and
73 confidence in predictions of the solid phases formed in the $\text{CaO-Al}_2\text{O}_3\text{-SiO}_2\text{-H}_2\text{O}$ system as simulated
74 by thermodynamic modelling. Hence, the development of thermodynamic models with explicit
75 descriptions of Al in C-A-S-H and C-(N-)A-S-H gels signifies an important advancement in how
76 cementitious materials are modelled and understood.

77

78 Here, a thermodynamic model is proposed to account explicitly for the tetrahedral Al and Na species
79 bound in C-(N-)A-S-H gel, and applied to simulate the chemistry of AAS cements as an initial
80 example. This model may also be applicable to high-volume blended PC/SCM materials (e.g. CEM III
81 blast furnace cements specified under the EN 197-1 standard) because the structurally-bound Al and
82 alkali species are specified independently in the model formulation, and because the C-(N-)A-S-H
83 and C-A-S-H gels formed in these materials and in AAS cements are similar in nanostructure and
84 chemical composition [26].

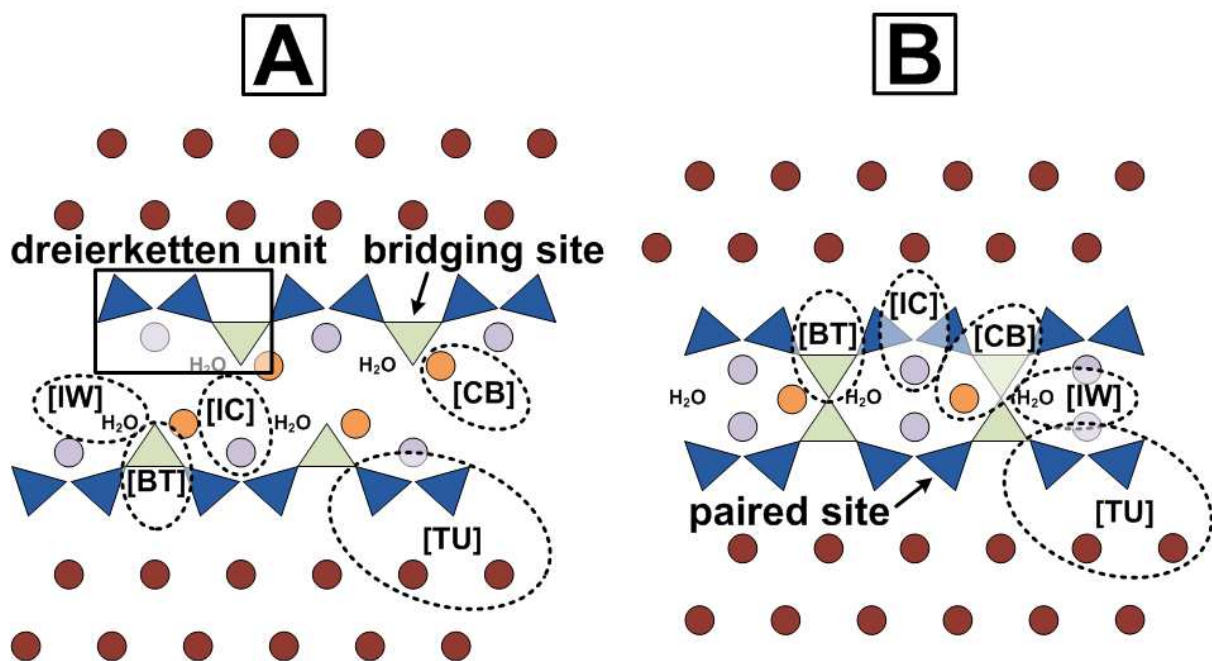
85

86

87 **2. The chemistry of AAS cements**

88

89 C-(N-)A-S-H gel, which is the dominant reaction product in AAS cements, contains aluminosilicate
90 chains arranged similarly to the disordered tobermorite-like phase C-S-H(I) [1], flanked on either side
91 by an 'interlayer' comprised of H₂O and aqueous cations (e.g. Ca²⁺), and a Ca-O sheet (Figure 1).
92 These aluminosilicate chains are comprised of substituted 'dreierketten' units, which are repeating
93 sets of three silicate tetrahedra (Figure 1). C-(N-)A-S-H gel is believed to exclude Al-O-Al bonding
94 [32], and to only contain significant Al substitution in the bridging tetrahedral sites defined in Figure
95 1, not in the paired sites [33]. The mean chain length (MCL) is defined here as the number of silicate
96 and aluminate tetrahedra per C-(N-)A-S-H chain. MCL values for C-(N-)A-S-H gels in alkali-activated
97 slag binders with KOH or NaOH activating solutions have been calculated to be between 4 and 8 [34-
98 37] using a non-crosslinked tobermorite/calcium hydroxide representation of this phase [38],
99 compared with 6-11 for C-(N-)A-S-H gels derived from slag reacted with sodium silicate activators
100 [39].
101



102
103 **Figure 1.** Schematic representations of infinite chain length non-crosslinked (A) and crosslinked (B)
104 C-(N-)A-S-H gel structures, with sublattice sites labelled: *TU*; *BT*; *CB*; *IC*; *IW*, as defined in the text
105 (eqs.(2,4)). Light green and dark blue triangles are paired and bridging tetrahedral sites respectively,
106 dark red circles represent Ca sites in the Ca-O sheets, and the orange and purple circles are positively

107 charged species (typically Ca^{2+} , H^+ , Na^+ and/or K^+) that charge-balance the aluminosilicate tetrahedra
108 in the *BT* and *TU* sites respectively.
109

110 Recent experimental results support a partially crosslinked structure for the C-(N-)A-S-H gel formed
111 in Na_2SiO_3 -activated slag binders: Q^3 type species have been identified in deconvolutions of ^{29}Si
112 magic angle spinning nuclear magnetic resonance (MAS NMR) spectra in silicate-activated slag
113 cements [39, 40] and in laboratory-synthesised gels [41, 42]. A mixed crosslinked/non-crosslinked
114 structural model was also needed to describe the mechanical properties of hydroxide and silicate-
115 activated slag cements [36].
116

117 The majority of AAS and related studies have used GBFS with Al_2O_3 content ≤ 14 wt.% and NaOH,
118 KOH or $\text{Na}_2\text{O}\cdot m\text{SiO}_2\cdot x\text{H}_2\text{O}$ activators. Most studies using NaOH or KOH solutions have reported Mg-
119 free binder compositions of $0.7 \leq \text{Ca}/\text{Si} \leq 1.2$ and $\text{Al}/\text{Si} \leq 0.25$ [35, 43-45], whereas those derived
120 from $\text{Na}_2\text{O}\cdot m\text{SiO}_2\cdot x\text{H}_2\text{O}$ solutions usually report Mg-free binder compositions of $0.6 \leq \text{Ca}/\text{Si} \leq 1.2$,
121 $\text{Al}/\text{Si} \leq 0.25$ [39, 40, 45, 46]. Laboratory-synthesised solids containing approximately phase-pure C-
122 (N-)A-S-H gels have typically shown chemical compositions of $0.5 < \text{Ca}/(\text{Al}+\text{Si}) \leq 1$ and $\text{Al}/\text{Si} \leq 0.20$
123 [42, 47, 48].
124

125 Bound water is present in variable amounts in the interlayer spacing in C-S-H type structures, with
126 $\text{H}_2\text{O}/\text{Si}$ ratios between 1.3-1.7 in gels with no adsorbed water [49], and must also be taken into
127 account in development of thermodynamic models for C-(N-)A-S-H gels. The amount of structurally
128 bound water in AAS cement is variable and not yet fully understood [50], so the water contents of
129 14\AA and 11\AA tobermorites may also be used to guide the development of thermodynamic models
130 for C-(N-)A-S-H gels. These minerals have bound $\text{H}_2\text{O}/\text{Si}$ ratios of 1.17 and 0.83 respectively [51, 52].
131
132

133 **3. Sublattice solid solution model for C-(N-)A-S-H gel**

134

135 **3.1 Sublattice solid solution definition**

136

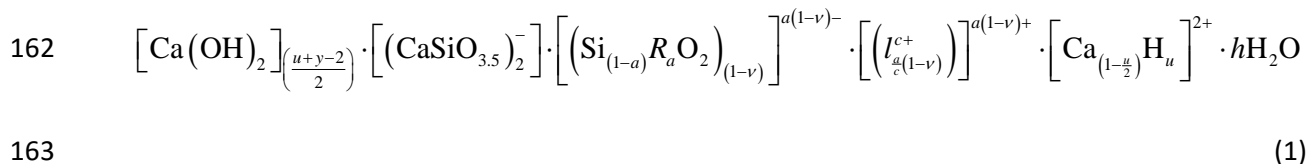
137 There exist several structural models that can describe C-S-H gels, as reviewed in detail by
138 Richardson [53, 54]. However, only the ‘Substituted General Model’ (SGM) [38] and the ‘Crosslinked
139 Substituted Tobermorite Model’ (CSTM) [39], can explicitly account for Al-substituted, alkali charge-
140 balanced structures such as C-(N-)A-S-H gel using a fully flexible formulation of the gel chemistry.
141 The CSTM describes C-(N-)A-S-H gel as a mixture of crosslinked and non-crosslinked tobermorite-like
142 structures, and is therefore more generalised than the SGM for systems containing $\text{Ca/Si} \leq 1.5$ (i.e.,
143 excluding solid solution $\text{Ca}(\text{OH})_2$). For $\text{Ca/Si} \leq 1.5$ the treatments of non-crosslinked C-(N-)A-S-H gel
144 components in the SGM and the CSTM are identical, with structural incorporation of Al and charge-
145 balancing by positively-charged interlayer species such as Na^+ . These structural models can be used
146 to constrain thermodynamic models because they provide a structurally-consistent basis from which
147 chemical compositions of C-(N-)A-S-H end-members can be determined.

148

149 Crosslinked and non-crosslinked C-(N-)A-S-H structures cannot always be distinguished from one
150 another by bulk chemical composition alone, which complicates the ability to differentiate between
151 these two structural types in thermodynamic models for this phase. Therefore, the SGM has been
152 used as a basis from which to derive the chemical composition of the C-(N-)A-S-H gel here explicitly
153 in terms of non-crosslinked structures, without precluding the possibility that the thermodynamic
154 model may also implicitly represent the bulk chemistry of crosslinked C-(N-)A-S-H gels. It is also
155 important to note that the C-S-H gel models derived by Kulik [25] used the ‘non-substituted general
156 model’ developed by Richardson and Groves [55], which is a simpler model related to the SGM. The
157 notation used by Kulik [25] and Richardson and Groves [38, 55] has been conserved where possible
158 for clarity.

159

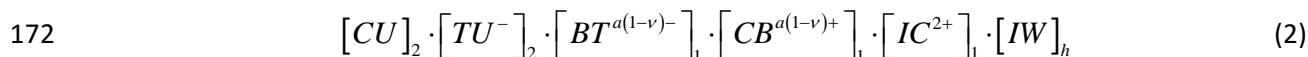
160 The SGM can be represented in terms of one dreierketten unit by eq.(1) (details of the derivation up
161 to this point are provided in Appendix A):



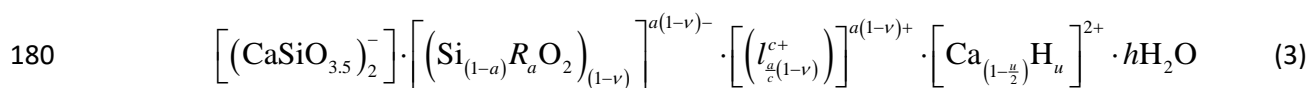
164 where R is a trivalent cation in tetrahedral coordination (e.g. Al^{3+}), I is a charge-balancing interlayer
165 cation (such as Na^+ , Ca^{2+} and/or H^+) with a positive charge of c , a is the extent of R substitution in
166 bridging sites (Figure 1), ν is the fraction of bridging site vacancies per dreierketten unit, u is the
167 interlayer H^+ content per dreierketten unit for the main chain sites (TU , $\text{CaSiO}_{3.5}^-$), and h defines the
168 amount of water per dreierketten unit. The SGM explicitly defines Al substitution in bridging sites
169 only, and excludes Al-O-Al bonding, consistent with Loewenstein's rule [32].

170

171 Eq.(1) can be equivalently written in sublattice notation as eq.(2):



173 where CU represents interstitial 'solid solution' $\text{Ca}(\text{OH})_2$ [55], BT are the bridging tetrahedra ($\text{Si}_{(1-
174 a)} R_a \text{O}_{2(1-\nu)}^{a(1-\nu)-}$), CB are the interlayer charge-balancing species for the bridging tetrahedra ($I_{a(1-\nu)/c}^{a(1-
175 \nu)+}$), IC are the interlayer charge-balancing species for the TU sites ($\text{Ca}_{(1-u/2)} \text{H}_u^{2+}$), and IW represents
176 interlayer water (H_2O). The CU sites in tobermorite are vacant (there is no interstitial 'solid solution'
177 $\text{Ca}(\text{OH})_2$), and are therefore eliminated from the structural definition in eqs.(1-2). This limits the
178 chemical composition of the sublattice solid solution model to $0.67 \leq \text{Ca}/\text{Si} \leq 1.5$ and leads to eqs.(3-
179 4):



181
$$\left[TU^- \right]_2 \cdot \left[BT^{a(1-\nu)^-} \right]_1 \cdot \left[CB^{a(1-\nu)^+} \right]_1 \cdot \left[IC^{2+} \right]_1 \cdot \left[IW \right]_h \quad (4)$$

182 This elimination of Ca(OH)₂ therefore provides the major limitation on the domain of applicability of
 183 the model described here; it is not able to be used for Ca/Si ratios > 1.5, but is valuable for alkali-
 184 activated cements and blended PC/SCM materials in which the composition of the C-(N-)A-S-H gel
 185 formed falls below this ratio. The sublattice sites shown in eq.(4) are illustrated in Figure 1.

186

187 The *IC* sites are now modified to enable the *TU* sites to be charge-balanced by Na⁺ species in
 188 addition to the *BT* sites. The possible interlayer charge-balancing species in C-(N-)A-S-H gel are not
 189 limited to Ca²⁺, H⁺ and Na⁺, but these are the only species for which sufficient data have been
 190 published to enable validation of the thermodynamic model developed here. Na-based solutions are
 191 also the most relevant alkaline activators for commercial use because they are relatively inexpensive
 192 and widely available [29]. The *BT* sites in C-(N-)A-S-H gel are mostly filled by vacancies, Si and/or Al
 193 species, meaning that *R* = Al can also be specified. Eq.(3) is re-written with the modified *IC* sites and
 194 with similarly modified *CB* sites, and with Al-substitution in the *BT* sites, which results in eq.(5):

195
$$\left[(CaSiO_{3.5})_2^- \right] \cdot \left[(Si_{(1-a)}Al_aO_2)_{(1-\nu)} \right]^{a(1-\nu)^-} \cdot \left[\left(Ca_{\left(\frac{1-d_1-d_2}{2}\right)} H_{d_1} Na_{d_2} \right)_{a(1-\nu)} \right]^{a(1-\nu)^+} \cdot \left[Ca_{\left(\frac{2-e_1-e_2}{2}\right)} H_{e_1} Na_{e_2} \right]^{2+} \cdot hH_2O \quad (5)$$

196

197 where $d_1 + d_2 \leq 1$ and $e_1 + e_2 \leq 2$.

198

199 While eqs.(4-5) are satisfactory for thermodynamic modelling, it is desirable to obtain a
 200 thermodynamic model which is consistent with existing validated formulations such as the
 201 downscaled CSH3T model [25]. In that model, the *BT*, *CB* and *IC* sites are combined into two
 202 potentially-equivalent *BCI* sites that could have different substitutions via the choice of two
 203 sublattice species, and the sublattice formula was 'downscaled' to 0.5 dreierketten units. The use of
 204 two such sites, rather than a single *BCI* site, is beneficial because it increases the number of unique
 205 chemical compositions that can be represented by the sublattice solid solution and can greatly

206 improve the fit of the thermodynamic model output to the validation data (e.g. solubility
 207 measurements) for the same set of mixing rules used (e.g. simple random ideal mixing). However,
 208 this means that end-member stoichiometries, and sublattice species and formulae are more likely to
 209 be represented in terms of fractional quantities rather than integer amounts. Fractional expressions
 210 obviously cannot directly correspond to atomistic-level structures, which means that
 211 thermodynamic models developed in this way can only describe the chemistry of solid solutions on
 212 the bulk scale rather than at the atomistic scale. Therefore, downscaling is useful in the
 213 development of thermodynamic models to describe complex phases such as C-(N-)A-S-H gels with
 214 atomistic structures that have not yet been fully resolved. Here, downscaling is essential to improve
 215 the number of unique chemical compositions and the volume of experimental data described by the
 216 sublattice solid solution model while keeping its formulation relatively simple, particularly because
 217 this model is required to describe C-(N-)A-S-H gel chemistry in the complex AAS cement system. The
 218 downscaled chemical and sublattice formulae (to 0.5 dreierketten units), written in terms of
 219 potentially-equivalent *BCI* sites ($BCI = BT + CB + IC$) and thus consistent with the downscaled
 220 CSH3T model [25], are shown in eqs.(6-7) respectively:

$$221 \quad [CaSiO_{3.5}]^- \cdot \left[\left\{ \left(Si_{(1-a)} Al_a O_2 \right)_{\frac{(1-\nu)}{2}} \cdot \left(Ca_{\left(\frac{1-d_1-d_2}{2}\right)} H_{d_1} Na_{d_2} \right)_{\frac{a(1-\nu)}{2}} \cdot \left(Ca_{\left(\frac{2-q-e_2}{2}\right)} H_{e_1} Na_{e_2} \right)_{\frac{1}{2}} \right\}^{\frac{0.5+}{2}} \right]_{\frac{1}{2}} \cdot \left[\left(\frac{h}{2} \right) H_2O \right]_{\frac{1}{2}} \quad (6)$$

$$223 \quad [TU^-]_1 \cdot [BCI^{0.5+}]_1 \cdot [BCI^{0.5+}]_1 \cdot [IW]_{\frac{h}{2}} \quad (7)$$

224
 225 Here, at least one additional (Al,Na)-containing sublattice species is necessary to represent C-(N-)A-
 226 S-H gel chemistry, compared to previous thermodynamic models for the CaO-SiO₂-H₂O system.
 227 Increasing the number of sublattice species and sites allows the description of a greater diversity of
 228 bulk C-(N-)A-S-H gel chemical compositions, and facilitates independent incorporation of Na and Al
 229 in C-S-H type structures. Additionally, as the quantities of bound water in C-(N-)A-S-H and C-S-H gels

230 are significantly different [50, 56], it is also necessary to allow for variation in the *IW* site. Here, C-(N-
 231)A-S-H gels are assumed to contain one mole of H₂O in the *IW* site per 0.5 dreierketten units (*h* = 2),
 232 because this is approximately equal to the chemistry of 11 Å and 14 Å tobermorites [51, 52] and the
 233 C-A-S-H type gels formed in AAS binders (H₂O/Si ≈ 1) [50].

234

235 These factors thus require the use of a sixth-order sublattice solid solution for the C-(N-)A-S-H
 236 thermodynamic model developed here. This solid solution contains five *BCI* sites, with each carrying
 237 a positive charge of 0.125 and grouped as shown in eqs.(8-9), and one variable *IW* site:

$$238 \left[\text{CaSiO}_{3.5} \right]^- \cdot [\text{H}_2\text{O}] \cdot \left[\left\{ \left(\text{Si}_{(1-a)}\text{Al}_a\text{O}_2 \right)_{\frac{(1-v)}{2}} \cdot \left(\text{Ca}_{\left(\frac{1-d_1-d_2}{2}\right)}\text{H}_{d_1}\text{Na}_{d_2} \right)_{\frac{a(1-v)}{2}} \cdot \left(\text{Ca}_{\left(\frac{2-e_1-e_2}{2}\right)}\text{H}_{e_1}\text{Na}_{e_2} \right)_{\frac{1}{2}} \right\}^{\frac{0.125+}{8}} \right] \cdot \left[\left(\frac{h}{2} - 1 \right) \text{H}_2\text{O} \right] \quad (8)$$

239

$$240 \left[\text{TU}^- \right]_1 \cdot [\text{IW}^*]_1 \cdot [\text{BCI}^{0.125+}]_2 \cdot [\text{BCI}^{0.125+}]_2 \cdot [\text{BCI}^{0.125+}]_2 \cdot [\text{BCI}^{0.125+}]_1 \cdot [\text{BCI}^{0.125+}]_1 \cdot [\text{IW}]_1 \quad (9)$$

241

242 where *IW** represents a fixed interlayer water site (with full occupancy of H₂O but otherwise
 243 identical to the *IW* site depicted in Figure 1). Eqs.(8-9) are the fundamental formulae that represent
 244 the C-(N-)A-S-H thermodynamic model developed here.

245

246 3.2 End-member selection

247

248 As discussed in section 1, a goal of this study is to develop a sublattice solid solution model that can
 249 describe the solubility and chemical composition of C-(N-)A-S-H gel in AAS cements. Based on the
 250 sublattice solid solution definition established in eqs.(8-9), it is now necessary to select a set of end-
 251 members, sublattice sites and species that can represent the chemistry of C-(N-)A-S-H gel.

252

253 Six species that can substitute into the five *BCI* sites given in eq.(9), and which are compatible with
 254 the chemical formula for these sites (eq.(8)) and the chemistry of C-(N-)A-S-H gels in AAS cements,
 255 were selected to represent a sublattice solid solution of the form shown in eq.(10):

$$256 \quad Q^* [A, B, C, D, E]_{\text{I}}^{n_1} [F, G, H, I, J]_{\text{II}}^{n_2} [K, L, M]_{\text{III}}^{n_3} [N, O, P, Q, R, S]_{\text{IV}}^{n_4} [T, U, V, W]_{\text{V}}^{n_5} [X, Y]_{\text{VI}}^{n_6} \quad (10)$$

257

258 Here, species *A, F, K, N, T* are $\text{Ca}_{0.0625}\text{O}_{0.0625}\text{H}_{0.125}^{0.125+}$, *B, G, L, O, U* are $\text{Si}_{0.0625}\text{O}_{0.125}\text{H}_{0.125}^{0.125+}$ and
 259 *D, I, M, Q, V* are $\text{Si}_{0.0625}\text{O}_{0.125}\text{Na}_{0.125}^{0.125+}$, which can be present in five different *BCI* sites, the species
 260 *C, H, P* are $\text{Al}_{0.0625}\text{O}_{0.125}\text{H}_{0.1875}^{0.125+}$ and *E, J, R* are $\text{Al}_{0.0625}\text{Na}_{0.0625}\text{O}_{0.125}\text{H}_{0.125}^{0.125+}$, which can fill four of
 261 the *BCI* sites, the species *S, W* are $\text{Ca}_{0.0625}\text{O}_{0.0625}\text{Na}_{0.125}^{0.125+}$, which can fill two of the *BCI* sites, *X* is
 262 H_2O , *Y* is a vacancy (V_{IW}), and Q^* is $\text{CaSiO}_{3.5}^- \cdot \text{H}_2\text{O}$. This combination of sublattice sites and species
 263 was chosen as it comprises the least complex formulation of the sublattice solid solution that can
 264 represent the chemistry of the C-(N-)A-S-H gel in AAS cements. In this work the coefficients $\text{I}=2$,
 265 $\text{II}=2$, $\text{III}=2$, $\text{IV}=1$, $\text{V}=1$ and $\text{VI}=1$ define the stoichiometry of the sublattice sites, and the
 266 superscripts n_1, n_2, n_3, n_4, n_5 and n_6 correspond to the five *BCI* sites and single *IW* site in eq.(9).
 267 Vacancies in *BCI* sites are included in the thermodynamic model via the ν parameter in eq.(8).

268

269 A minimal set of eight end-members was chosen within this sublattice solid solution model to define
 270 the C-(N-)A-S-H gel in this work, as shown in Table 1. This is the smallest number of end-members
 271 that can resemble the chemistry of C-(N-)A-S-H gels (section 2) and describe the available solubility
 272 data for AAS cement and the $\text{CaO}-(\text{Na}_2\text{O}, \text{Al}_2\text{O}_3)-\text{SiO}_2-\text{H}_2\text{O}$ systems (section 6). The solid solution
 273 contains three C-S-H end-members, one C-(N-)S-H end-member, two C-A-S-H end-members and two
 274 C-(N-)A-S-H end-members. The C-S-H end-members have the same chemical compositions as the
 275 T2C, T5C and TobH end-members of the downscaled CSH3T model (T2C*, T5C* and TobH*
 276 respectively) [25], which contain the *TU* site, $h = 4$, and two *BCI* sublattice species, $\text{Si}_{0.25}\text{O}_{0.5}\text{H}_{0.5}^+$
 277 and $\text{Ca}_{0.25}\text{O}_{0.25}\text{H}_{0.5}^+$, for $a = 0$, to cover the range $0.67 \leq \text{Ca}/\text{Si} \leq 1.5$ in the $\text{CaO}-\text{SiO}_2-\text{H}_2\text{O}$ system. One

This paper was published in *Cement and Concrete Research*, 66(2014):27-47. The version of record is available at <http://dx.doi.org/10.1016/j.cemconres.2014.07.005>

278 H₂O molecule is also added per vacancy in the bridging tetrahedra for each of the eight end-
279 members (determined by the value of ν).

280

281 **Table 1.** Chemical compositions of the eight end-members of the C-(N)-A-S-H thermodynamic model, and parameters chosen for use in eq.(8). One H₂O
 282 molecule is added to the *BCI* site per bridging site vacancy for consistency with the C-S-H thermodynamic model developed by Kulik [25].

End-member	ν	a	i_1	i_2	u_1	u_2	M	Sublattice formula ^b	Chemical formula
5CA	0.5	1	1	0	1	0	2	$[(\text{CaSiO}_{3.5})^-]_1 \cdot [\text{H}_2\text{O}]_1 \cdot [\text{Al}_{0.0625}\text{O}_{0.125}\text{H}_{0.1875}^{0.125+}]_2 \cdot [\text{Al}_{0.0625}\text{O}_{0.125}\text{H}_{0.1875}^{0.125+}]_2 \cdot [\text{Ca}_{0.0625}\text{O}_{0.0625}\text{H}_{0.125}^{0.125+}]_2 \cdot [\text{Ca}_{0.0625}\text{O}_{0.0625}\text{H}_{0.125}^{0.125+}]_1 \cdot [\text{Ca}_{0.0625}\text{O}_{0.0625}\text{H}_{0.125}^{0.125+}]_1 \cdot [\text{V}_{\text{H}_2\text{O}}]_1$	$(\text{CaO})_{1.25}(\text{Al}_2\text{O}_3)_{0.125}(\text{SiO}_2)_1(\text{H}_2\text{O})_{1.625}$
INFCA	0	0.625	1	0	2	0	2	$[(\text{CaSiO}_{3.5})^-]_1 \cdot [\text{H}_2\text{O}]_1 \cdot [\text{Al}_{0.0625}\text{O}_{0.125}\text{H}_{0.1875}^{0.125+}]_2 \cdot [\text{Al}_{0.0625}\text{O}_{0.125}\text{H}_{0.1875}^{0.125+}]_2 \cdot [\text{Si}_{0.0625}\text{O}_{0.125}\text{H}_{0.125}^{0.125+}]_2 \cdot [\text{Al}_{0.0625}\text{O}_{0.125}\text{H}_{0.1875}^{0.125+}]_1 \cdot [\text{Si}_{0.0625}\text{O}_{0.125}\text{H}_{0.125}^{0.125+}]_1 \cdot [\text{V}_{\text{H}_2\text{O}}]_1$	$(\text{CaO})_1(\text{Al}_2\text{O}_3)_{0.15625}(\text{SiO}_2)_{1.1875}(\text{H}_2\text{O})_{1.65625}$
5CNA	0.5	1	0	1	0.5	0.5	2	$[(\text{CaSiO}_{3.5})^-]_1 \cdot [\text{H}_2\text{O}]_1 \cdot [\text{Al}_{0.0625}\text{Na}_{0.0625}\text{O}_{0.125}\text{H}_{0.125}^{0.125+}]_2 \cdot [\text{Al}_{0.0625}\text{Na}_{0.0625}\text{O}_{0.125}\text{H}_{0.125}^{0.125+}]_2 \cdot [\text{Ca}_{0.0625}\text{O}_{0.0625}\text{H}_{0.125}^{0.125+}]_2 \cdot [\text{Ca}_{0.0625}\text{O}_{0.0625}\text{Na}_{0.125}^{0.125+}]_1 \cdot [\text{Ca}_{0.0625}\text{O}_{0.0625}\text{Na}_{0.125}^{0.125+}]_1 \cdot [\text{V}_{\text{H}_2\text{O}}]_1$	$(\text{CaO})_{1.25}(\text{Na}_2\text{O})_{0.25}(\text{Al}_2\text{O}_3)_{0.125}(\text{SiO}_2)_1(\text{H}_2\text{O})_{1.375}$
INFCNA	0	0.625	0	1	1.25	0.75	2	$[(\text{CaSiO}_{3.5})^-]_1 \cdot [\text{H}_2\text{O}]_1 \cdot [\text{Al}_{0.0625}\text{Na}_{0.0625}\text{O}_{0.125}\text{H}_{0.125}^{0.125+}]_2 \cdot [\text{Al}_{0.0625}\text{Na}_{0.0625}\text{O}_{0.125}\text{H}_{0.125}^{0.125+}]_2 \cdot [\text{Si}_{0.0625}\text{O}_{0.125}\text{Na}_{0.125}^{0.125+}]_2 \cdot [\text{Al}_{0.0625}\text{Na}_{0.0625}\text{O}_{0.125}\text{H}_{0.125}^{0.125+}]_1 \cdot [\text{Si}_{0.0625}\text{O}_{0.125}\text{Na}_{0.125}^{0.125+}]_1 \cdot [\text{V}_{\text{H}_2\text{O}}]_1$	$(\text{CaO})_1(\text{Na}_2\text{O})_{0.34375}(\text{Al}_2\text{O}_3)_{0.15625}(\text{SiO}_2)_{1.1875}(\text{H}_2\text{O})_{1.3125}$
INFCN	0	0	1	0	0.75	1.25	2	$[(\text{CaSiO}_{3.5})^-]_1 \cdot [\text{H}_2\text{O}]_1 \cdot [\text{Si}_{0.0625}\text{O}_{0.125}\text{Na}_{0.125}^{0.125+}]_2 \cdot [\text{Si}_{0.0625}\text{O}_{0.125}\text{Na}_{0.125}^{0.125+}]_2 \cdot [\text{Si}_{0.0625}\text{O}_{0.125}\text{Na}_{0.125}^{0.125+}]_1 \cdot [\text{Si}_{0.0625}\text{O}_{0.125}\text{H}_{0.125}^{0.125+}]_1 \cdot [\text{V}_{\text{H}_2\text{O}}]_1$	$(\text{CaO})_1(\text{Na}_2\text{O})_{0.3125}(\text{SiO}_2)_{1.5}(\text{H}_2\text{O})_{1.1875}$
T2C* ^a	1	0	0	0	0	0	4	$[(\text{CaSiO}_{3.5})^-]_1 \cdot [\text{H}_2\text{O}]_1 \cdot [\text{Ca}_{0.0625}\text{O}_{0.0625}\text{H}_{0.125}^{0.125+}]_2 \cdot [\text{Ca}_{0.0625}\text{O}_{0.0625}\text{H}_{0.125}^{0.125+}]_2 \cdot [\text{Ca}_{0.0625}\text{O}_{0.0625}\text{H}_{0.125}^{0.125+}]_1 \cdot [\text{Ca}_{0.0625}\text{O}_{0.0625}\text{H}_{0.125}^{0.125+}]_1 \cdot [\text{H}_2\text{O}]_1$	$(\text{CaO})_{1.5}(\text{SiO}_2)_1(\text{H}_2\text{O})_{2.5}$
T5C* ^a	0.5	0	0	0	1	0	4	$[(\text{CaSiO}_{3.5})^-]_1 \cdot [\text{H}_2\text{O}]_1 \cdot [\text{Si}_{0.0625}\text{O}_{0.125}\text{H}_{0.125}^{0.125+}]_2 \cdot [\text{Si}_{0.0625}\text{O}_{0.125}\text{H}_{0.125}^{0.125+}]_2 \cdot [\text{Ca}_{0.0625}\text{O}_{0.0625}\text{H}_{0.125}^{0.125+}]_2 \cdot [\text{Ca}_{0.0625}\text{O}_{0.0625}\text{H}_{0.125}^{0.125+}]_1 \cdot [\text{Ca}_{0.0625}\text{O}_{0.0625}\text{H}_{0.125}^{0.125+}]_1 \cdot [\text{H}_2\text{O}]_1$	$(\text{CaO})_{1.25}(\text{SiO}_2)_{1.25}(\text{H}_2\text{O})_{2.5}$
TobH* ^a	0	0	0	0	2	0	4	$[(\text{CaSiO}_{3.5})^-]_1 \cdot [\text{H}_2\text{O}]_1 \cdot [\text{Si}_{0.0625}\text{O}_{0.125}\text{H}_{0.125}^{0.125+}]_2 \cdot [\text{Si}_{0.0625}\text{O}_{0.125}\text{H}_{0.125}^{0.125+}]_2 \cdot [\text{Si}_{0.0625}\text{O}_{0.125}\text{H}_{0.125}^{0.125+}]_1 \cdot [\text{Si}_{0.0625}\text{O}_{0.125}\text{H}_{0.125}^{0.125+}]_1 \cdot [\text{H}_2\text{O}]_1$	$(\text{CaO})_1(\text{SiO}_2)_{1.5}(\text{H}_2\text{O})_{2.5}$

283 ^a The asterisks for the T2C*, T5C* and TobH* end-members indicate that these components have the same bulk chemistry but slightly modified
 284 thermodynamic properties relative to the T2C, T5C and TobH end-members of the downscaled CSH3T model [25].

285 ^b V_{H₂O} is a vacancy in the *IW* sublattice site.

286 As each species (A to Y) is defined to only substitute into one site (i.e., species with the same
 287 chemistry but occupying different sites are treated as being distinct), the site fraction of a species i
 288 in a given site n_s , $y_i^{n_s}$, is defined as $y_i^{n_s} = \sum (\chi_k^{i,n_s})$ for $\sum (y_i^{n_s}) = 1$. Here $n_s \in \{n_1, n_2, n_3, n_4, n_5, n_6\}$
 289 is the sublattice site, χ_k^{i,n_s} is the effective mole fraction of end-member k containing the species i in
 290 the sublattice site n_s , with $\sum_k (\chi_k) = 1$. In defining an end-member of the sublattice solid solution
 291 model, the species present in the s^{th} sublattice site may be identified by the same subscript number
 292 i.e. i_l is the species present in the sublattice site n_l , and $i_l \in \{A, B, C, D, E\}$. Thus an end-member
 293 can be equivalently written in terms of its substituting species, i.e. $k = i_1 i_2 i_3 \dots i_s$.

294

295 The chain length (CL) for each of the end-members, and the MCL of the C-(N)-A-S-H gel as a whole,
 296 can then be calculated from eq.(11).

297
$$CL = \frac{3}{\sum_k (\chi_k \nu_k)} - 1 \quad (11)$$

298

299 The fraction of bridging site vacancies per dreierketten unit, ν , is shown in Table 1 for each end-
 300 member of the C-(N)-A-S-H thermodynamic model. This equation represents the minimum chain
 301 length possible for the end-members, and thus the minimum MCL of the C-(N)-A-S-H gel, because
 302 eq.(11) implies that the end-members are strictly non-crosslinked. The chain lengths of crosslinked
 303 C-(N)-A-S-H end-members would be calculated in the same way, but with a factor of two included
 304 (i.e. $CL_{crosslinked} = 2CL$) to reflect the double chain structures in these phases. Here, these crosslinked
 305 and non-crosslinked structures were not explicitly differentiated in defining the end-members
 306 (eqs.(8-9)), meaning that eq.(11) provides a lower bound on the MCLs of partially (or fully)
 307 crosslinked C-(N)-A-S-H gels.

308

4. Thermodynamic basis of the sublattice solid solution model

309
310

311 The chemical potential (partial molal Gibbs free energy), $\mu_{i_1 i_2 i_3 \dots i_s}$, of end-member $i_1 i_2 i_3 \dots i_s$ in a multi-
312 component solid solution can be represented by eq.(12) [57]:

$$\mu_{i_1 i_2 i_3 \dots i_s} = G_m + \left[\frac{\partial G_m}{\partial y_{i_1}^{n_1}} + \frac{\partial G_m}{\partial y_{i_2}^{n_2}} + \frac{\partial G_m}{\partial y_{i_3}^{n_3}} + \dots + \frac{\partial G_m}{\partial y_{i_s}^{n_s}} \right] - \left[\sum_i \left(y_i \frac{\partial G_m}{\partial y_i} \right) \right] \quad (12)$$

314 where G_m is the Gibbs free energy of mixing using the notation previously introduced, and can be
315 expressed by eq.(13) [58]:

$$G_m = G^{mech} - TS_m^{id} + G_m^E \quad (13)$$

317 where G^{mech} is the Gibbs free energy of a compositionally-equivalent ‘mechanical mixture’ of simple
318 components to the solid solution phase, S_m^{id} is the difference in entropy between the ideal solid
319 solution for the solid phase and its end-member components (i.e. the configurational entropy), and
320 G_m^E is the excess Gibbs free energy of mixing (representing the deviation of the solid solution from
321 ideality).

322

323 Here, the ‘compound energy formalism’ is used to define the surface of reference for the Gibbs free
324 energy of mixing as a weighted average of the Gibbs free energy of each of the (pure) end-members
325 in the C-(N-)A-S-H solid solution [57]. This is formally expressed by eq.(14) for a multi-site, multi-
326 component sublattice solid solution, assuming random mixing within each sublattice [59]:

$$G_m = \left[\sum_{n_1} \sum_{n_2} \sum_{n_3} \dots \sum_{n_s} \left(y_{i_1}^{n_1} y_{i_2}^{n_2} y_{i_3}^{n_3} \dots y_{i_s}^{n_s} \right) {}^o G_{i_1 i_2 i_3 \dots i_s} \right] + R^* T \left[\text{I} \sum_{i_1} \left(y_{i_1} \ln y_{i_1} \right) + \text{II} \sum_{i_2} \left(y_{i_2} \ln y_{i_2} \right) + \text{III} \sum_{i_3} \left(y_{i_3} \ln y_{i_3} \right) + \dots + \zeta \sum_{i_s} \left(y_{i_s} \ln y_{i_s} \right) \right] + G_m^E \quad (14)$$

328

329 where ${}^{\circ}G_{i_1i_2i_3\cdots i_s}$ is the standard Gibbs free energy of end-member $i_1i_2i_3\cdots i_s$, R^* is the universal gas
 330 constant, T is temperature and ζ is the stoichiometric coefficient of the s^{th} sublattice site. The
 331 random mixing assumption is appropriate here because it greatly simplifies the expression for the
 332 configurational entropy and because the solid solution definition (eqs.(8-9)) does not represent
 333 atomic-scale structures; assigning hypothetical weightings to non-physical mixing combinations
 334 would not make physical sense. This choice is reasonable given that this is the first attempt to
 335 develop a sublattice solid solution model for C-(N-)A-S-H gel, and will be validated in section 6
 336 through the ability of the model to accurately describe chemical composition and solubility data for
 337 this phase.

338

339 Eq.(14) can be expanded explicitly for the sublattice solid solution defined by the eight end-members
 340 shown in Table 1. Substituting this expanded version of eq.(14) into eq.(12), defining a generalised
 341 end-member with species A, F, K, N, T, X in sublattice sites $n_1, n_2, n_3, n_4, n_5, n_6$ and then simplifying,
 342 results in eq.(15):

$$343 \quad \mu_{AFKNTX} = {}^{\circ}G_{AFKNTX} + RT \left[2 \ln(y_A) + 2 \ln(y_F) + 2 \ln(y_K) + \ln(y_N) + \ln(y_T) + \ln(y_X) \right] + G_m^E + U \quad (15)$$

344

345 Equivalent relationships for μ_{AFKNTX} can be written for all other combinations of sublattice site
 346 occupancies. The U term contains the Gibbs free energies for the reciprocal reactions ($\Delta_{rcp}{}^{\circ}G$), which
 347 denotes the difference in Gibbs free energy between combinations of end-members in the sublattice
 348 solid solution (which must by definition contain equal numbers of reactant and product terms). For
 349 example, the reciprocal reaction (eq.(16)) has a corresponding Gibbs free energy of reaction given by
 350 eq.(17):



$$352 \quad \Delta_{rcp}{}^{\circ}G_{LO} = {}^{\circ}G_{AFKOTX} + {}^{\circ}G_{AFLNTX} - {}^{\circ}G_{AFKNTX} - {}^{\circ}G_{AFLOTX} \quad (17)$$

353

354 It is possible to make two key simplifications here. The first is setting $G_m^E = 0$, i.e. interactions
355 between atoms in the same sublattice sites are neglected, meaning that the sublattice solid solution
356 model is ideal. The second is that the Gibbs free energies of the reciprocal reactions in the solid
357 solution are numerically approximated to zero ($U = 0$). The reciprocal reaction terms describe the
358 nearest-neighbour interactions in the solid solution, so are likely to influence end-member chemical
359 potentials more than the next-nearest-neighbour interactions described by the excess Gibbs free
360 energy terms. These terms are likely to be non-zero in C-(N-)A-S-H gels, because it is known that
361 thermodynamic energetic differences arise from nearest-neighbour Si-Al substitution in
362 aluminosilicate systems [60], but this approach can be validated by the good fit of the
363 thermodynamic model to the published solubility and chemical composition data in the CaO-
364 (Na₂O,Al₂O₃)-SiO₂-H₂O systems (section 6). In defining the mixing rules in this way, the accuracy of
365 the thermodynamic model is determined semi-empirically through the use of end-members with
366 carefully selected chemical compositions and Gibbs free energies that internalise the nearest and
367 next-nearest neighbour interactions in C-(N-)A-S-H gels, rather than through the explicit definition of
368 these interactions. However, quantification of these interactions in terms of chemical potentials for
369 hypothetical C-(N-)A-S-H end-members, and a better understanding of the solubility of C-(N-)A-S-H
370 gels, will be important future steps in the model development.

371

372 Application of these assumptions to eq.(15) leads to the final, simplified formula for the chemical
373 potential of an end-member in the C-(N-)A-S-H sublattice solid solution model (eq.(18)):

374
$$\mu_{AFKNTX} = {}^oG_{AFKNTX} + RT \left[2\ln(y_A) + 2\ln(y_F) + 2\ln(y_K) + \ln(y_N) + \ln(y_T) + \ln(y_X) \right] \quad (18)$$

375

376 The C-(N-)A-S-H thermodynamic model developed here is implemented in the GEM-Selektor v3
377 thermodynamic modelling software (<http://gems.web.psi.ch/>) [61, 62]. Sublattice solid solution
378 models can be specified in GEM-Selektor by modifying the activities of the chosen end-members

379 (Table 1) through the introduction of a ‘fictive activity coefficient’ λ , which internalises the
380 thermodynamic mixing relationships within the solid solution. This method was used in the C-S-H
381 thermodynamic model developed by Kulik [25]. The fictive activity coefficient is defined by eq.(19):

$$382 \quad \lambda_k = \frac{\alpha_k}{\chi_k} \quad (19)$$

383 where α_k is the activity of the k^{th} end-member, eq.(20):

$$384 \quad \mu_k = \mu_k^o + RT \ln(\alpha_k) \quad (20)$$

385

386 The fictive activity coefficient is defined by eliminating μ_k and the ${}^oG_{AFKNTX}$ term (equivalent to μ_k^o as
387 defined here) from eqs.(18,20), then substituting eq.(19) into the resulting equation and simplifying
388 to obtain eq.(21):

$$389 \quad \ln(\lambda_{AFKNTX}) = \left[2 \ln(y_A) + 2 \ln(y_F) + 2 \ln(y_K) + \ln(y_N) + \ln(y_T) + \ln(y_X) \right] \\ - \ln(\chi_{AFKNTX}) \quad (21)$$

390 Relationships equivalent to eq.(21) can thus be obtained for all eight end-members (Table 1). The
391 fictive activity coefficient relationships for these end-members are shown in Appendix B.

392

393

394 **5. Modelling method**

395

396 **5.1 Modelling system definition**

397 The kernel Nagra/PSI [63], which is the default thermodynamic database for GEM-Selektor v3
398 (<http://gems.web.psi.ch/>) [61, 62], and the CEMDATA07 thermodynamic database [17, 23, 64-69],
399 which contains data for various compounds commonly found in cement systems, were used during
400 simulations. The ideal gas equation of state is used to describe the gases and the Truesdell-Jones
401 form of the extended Debye-Hückel equation, eq.(22) [70], is used to describe the aqueous species.

402
$$\log_{10} \gamma_j = \frac{-A_\gamma z_j^2 \sqrt{I}}{1 + a B_\gamma \sqrt{I}} + b_\gamma I + \log_{10} \frac{x_{jw}}{X_w} \quad (22)$$

403

404 Here, γ_j and z_j are the activity coefficient and charge of the j^{th} aqueous species respectively, A_γ and B_γ
405 are temperature and pressure-dependent electrostatic parameters, I is the ionic strength of the
406 aqueous electrolyte phase, a is the ion size parameter, b_γ is a parameter that describes short-range
407 interactions between charged aqueous species in an electrolyte solution (representing the
408 predominant electrolyte in the system), x_{jw} is the molar quantity of water, and X_w is the total molar
409 amount of the aqueous phase. Constant values of a (3.31 Å) and b_γ (0.098 kg/mol) are taken to
410 represent the average ion size and common short-range interactions of charged aqueous species in a
411 NaOH-dominated solution [70]. The water activity is calculated from the osmotic coefficient [70].

412

413 The extended Debye-Hückel equation is accurate at moderate ionic strengths (up to ~ 1 molal) [70],
414 which is lower than the ionic strength in AAS pore solutions (~1-3 molal in sodium silicate activated
415 slag cements, e.g. [71]), but this equation was chosen here as a first step in development of the
416 thermodynamic model as it is directly encoded in GEM-Selektor. Additionally, the description of
417 aqueous silicate speciation in the GEM-Selektor databases does not currently extend beyond dimeric
418 silicate and aluminosilicate units, and adsorption of aqueous species onto simulated solid phases is
419 also not fully taken into account. Use of an improved aqueous phase model, such as the Pitzer model
420 [72] coupled with a more complete description of silicate oligomerisation [73], and description of
421 sorption effects, are goals of future work.

422

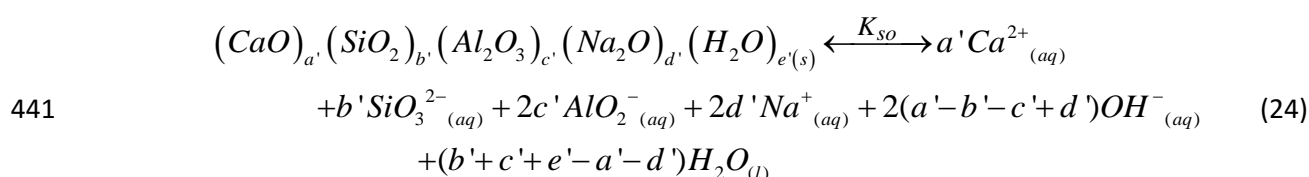
423 **5.2 Thermodynamic property estimation**

424 The standard absolute isobaric heat capacity (C_p°) and absolute entropy at standard state (S°) of the
425 five (Al,Na)-containing C-(N-)A-S-H end-members were estimated using the additivity method and
426 eq.(23), defined in terms of structurally-relevant constituents: T2C (the Ca-rich end-member of the

427 downscaled CSH3T model [25], $(CaO)_{1.5}(SiO_2)_1(H_2O)_{2.5}$, portlandite $(Ca(OH)_2)$, amorphous SiO_2 ,
 428 gibbsite $(Al(OH)_3)$ and $NaOH_{(s)}$.

$$\begin{aligned} \Phi^o_{(CaO)_a'(SiO_2)_b'(Al_2O_3)_c'(Na_2O)_d'(H_2O)_e'} &= \frac{1}{2}(5a' - 3e' + 9c' + 3d')\Phi^o_{Ca(OH)_2} \\ &+ (b' - e' + a' + 3c' + d')\Phi^o_{SiO_2} + 2c'\Phi^o_{Al(OH)_3} + 2d'\Phi^o_{NaOH} \\ &+ (e' - a' - 3c' - d')\Phi^o_{(CaO)_{1.5}(SiO_2)_1(H_2O)_{2.5}} \end{aligned} \quad (23)$$

430
 431 Here Φ^o denotes the standard thermodynamic property undergoing estimation (Cp^o or S^o), a' , b' , c' ,
 432 d' , e' are the stoichiometric coefficients for the respective oxide components CaO , SiO_2 , Al_2O_3 ,
 433 Na_2O and H_2O , and the numerical coefficients for these terms are the values that result from solving
 434 the elemental balance for eq.(23). The thermodynamic properties of the constituent phases are
 435 provided in Appendix C, and are consistent with the Nagra/PSI [63] and CEMDATA07 thermodynamic
 436 databases [17, 23, 64-69]. The additivity method is expected to yield relatively small errors in
 437 estimated values for Cp^o and S^o if suitable constituents are chosen [74]. The changes in S^o and Cp^o ,
 438 and the solubility product (K_{so}) of the (Al,Na)-containing C-(N)-A-S-H end-members for the
 439 dissociation reaction represented by eq.(24), were determined to enable thermodynamic property
 440 calculations in GEM-Selektor:



442
 443 The ReacDC module in GEM-Selektor was used to determine the standard partial molal Gibbs free
 444 energies ($\Delta_f G^o$) and enthalpies of formation ($\Delta_f H^o$) for the proposed C-(N)-A-S-H end-members by
 445 specifying 'optimised' solubility products for the reaction shown in eq.(24), the value of S^o
 446 determined via the additivity method (using the components listed previously), and the change in S^o
 447 of the dissociation reaction (eq.(24)). The Gibbs free energies (and thus the enthalpies) of the T2C*,

448 T5C* and TobH* end-members were modified slightly from the values reported in the downscaled
 449 CSH3T model [25], and solubility products of the (Al,Na)-containing C-(N)-A-S-H end-members were
 450 selected, to obtain the optimised fit of the thermodynamic model to the solubility and solid phase
 451 chemistry data in the CaO-(Na₂O,Al₂O₃)-SiO₂-H₂O [2-15, 41, 42, 48, 75-81] and AAS cement systems
 452 [71, 82-84] used in model validation (section 6). All other thermodynamic parameters of the T2C*,
 453 T5C* and TobH* end-members were adopted directly from the downscaled CSH3T model.

454
 455 Standard molar volumes (V^o) of the (Al,Na)-containing C-(N)-A-S-H end-members were determined
 456 from density calculations using the method proposed by Thomas et al. [50], but extended to include
 457 Na species via eq.(25):

$$458 \quad \rho^{sc}_{CNASH} = N_A \rho'_{CNASH} \left[\frac{\left(\frac{CaO}{SiO_2}\right) b^{sc}_{CaO} + b^{sc}_{SiO_2} + \left(\frac{Al_2O_3}{SiO_2}\right) b^{sc}_{Al_2O_3} + \left(\frac{Na_2O}{SiO_2}\right) b^{sc}_{Na_2O} + \left(\frac{H_2O}{SiO_2}\right) b^{sc}_{H_2O}}{MW_{CNASH}} \right] \quad (25)$$

459 where the b^{sc} parameters are the established neutron scattering lengths for CaO, SiO₂, Al₂O₃, Na₂O
 460 and H₂O, ρ^{sc} is the scattering length density taken from the literature [50], ρ'_{CNASH} is the predicted
 461 density of a C-(N)-A-S-H end-member, N_A is Avogadro's number, MW_{CNASH} is the molecular weight of
 462 a C-(N)-A-S-H end-member, and the ratios CaO/SiO₂, Al₂O₃/SiO₂, Na₂O/SiO₂, and H₂O/SiO₂ are molar
 463 composition ratios of a C-(N)-A-S-H end-member. The optimised thermodynamic properties for the
 464 C-(N)-A-S-H end-members are summarised in Table 2.

465

466 **Table 2.** Thermodynamic properties, densities and the change in thermodynamic properties for the
 467 dissociation reaction (eq.(24)) for the end-members of the C-(N)-A-S-H solid solution (25°C, 1 bar)

Standard thermodynamic properties and density						
End-member	V^o (cm ³ /mol)	$\Delta_f H^o$ (kJ/mol)	$\Delta_f G^o$ (kJ/mol)	S^o (J/mol.K)	C_p^o (J/mol.K)	ρ'_{CNASH} (g/cm ³)
5CA	57.3	-2491	-2293	163	177	3.01
INFCA	59.3	-2551	-2343	154	181	2.92
5CNA	64.5	-2569	-2382	195	176	2.84
INFCNA	69.3	-2667	-2474	198	180	2.72
INFCN	71.1	-2642	-2452	186	184	2.63
T2C* ^a	80.6	-2721	-2465	167	237	2.35
T5C* ^a	79.3	-2780	-2517	160	234	2.40

TobH* ^a	85.0	-2831	-2560	153	231	2.25
Change in thermodynamic properties for the dissociation reaction (eq.(24))						
End-member	$\Delta_r V^\circ$ (cm ³ /mol)	$\Delta_r H^\circ$ (kJ/mol)	$\Delta_r G^\circ$ (kJ/mol)	$\Delta_r S^\circ$ (J/mol.K)	$\Delta_r Cp^\circ$ (J/mol.K)	$\log_{10}(K_{so})$
5CA	-17.9	-4.0	61.4	-219	-29.3	-10.75
INFCA	5.1	0.58	50.8	-168	160	-8.90
5CNA	-37.1	-18.8	59.4	-262	-115	-10.4
INFCNA	-21.3	-10.8	57.1	-228	41.5	-10.0
INFCN	-12.5	-6.2	61.1	-226	144	-10.7

468 ^a The $\log_{10}(K_{so})$ values for the T2C*, T5C* and TobH* end-members, for the dissociation reaction
469 eq.(24), are -11.6, -10.5 and -7.9 respectively.

470

471

472 6. Application of the thermodynamic model in GEM-Selektor

473

474 6.1 Approach

475 The success of a thermodynamic model is measured in terms of its ability to describe the available
476 thermochemical data in the target system(s) - here, for Ca-rich alkali-activated cements such as AAS
477 cements and hybrid alkali-activated/PC materials - and its ability to predict the chemistry of
478 simulated systems where experimental data are either not available or are difficult to obtain. Hence,
479 thermodynamic models for cements must be developed using existing experimental results such as
480 solubility measurements [8, 47], solid product assemblages [35, 37, 43], and/or the chemistry of C-
481 (N-)A-S-H gels [42]. An extensive set of experimental solubility data in the CaO-SiO₂-H₂O system is
482 available for the development of thermodynamic models for C-S-H gels [2-15], but the use of such
483 information to develop models for C-(N-)A-S-H gels is significantly more complicated. Solubility
484 measurements in the CaO-Na₂O-Al₂O₃-SiO₂-H₂O system are not available in sufficient detail to enable
485 development of thermodynamic models using this information alone, meaning that validation
486 against other data is necessary. In this light, AAS cements provide an opportunity to validate the
487 thermodynamic model; these materials are described mostly in terms of the more complex CaO-
488 Na₂O-Al₂O₃-SiO₂-H₂O-MgO system, but are relatively well characterised. Hence, the thermodynamic

489 model here is validated for the less complex $\text{CaO}-(\text{Na}_2\text{O},\text{Al}_2\text{O}_3)\text{-SiO}_2\text{-H}_2\text{O}$ systems, and also AAS
490 cements. The ability of the thermodynamic model to predict solid phase assemblages in these
491 systems will be discussed in a subsequent publication.

492

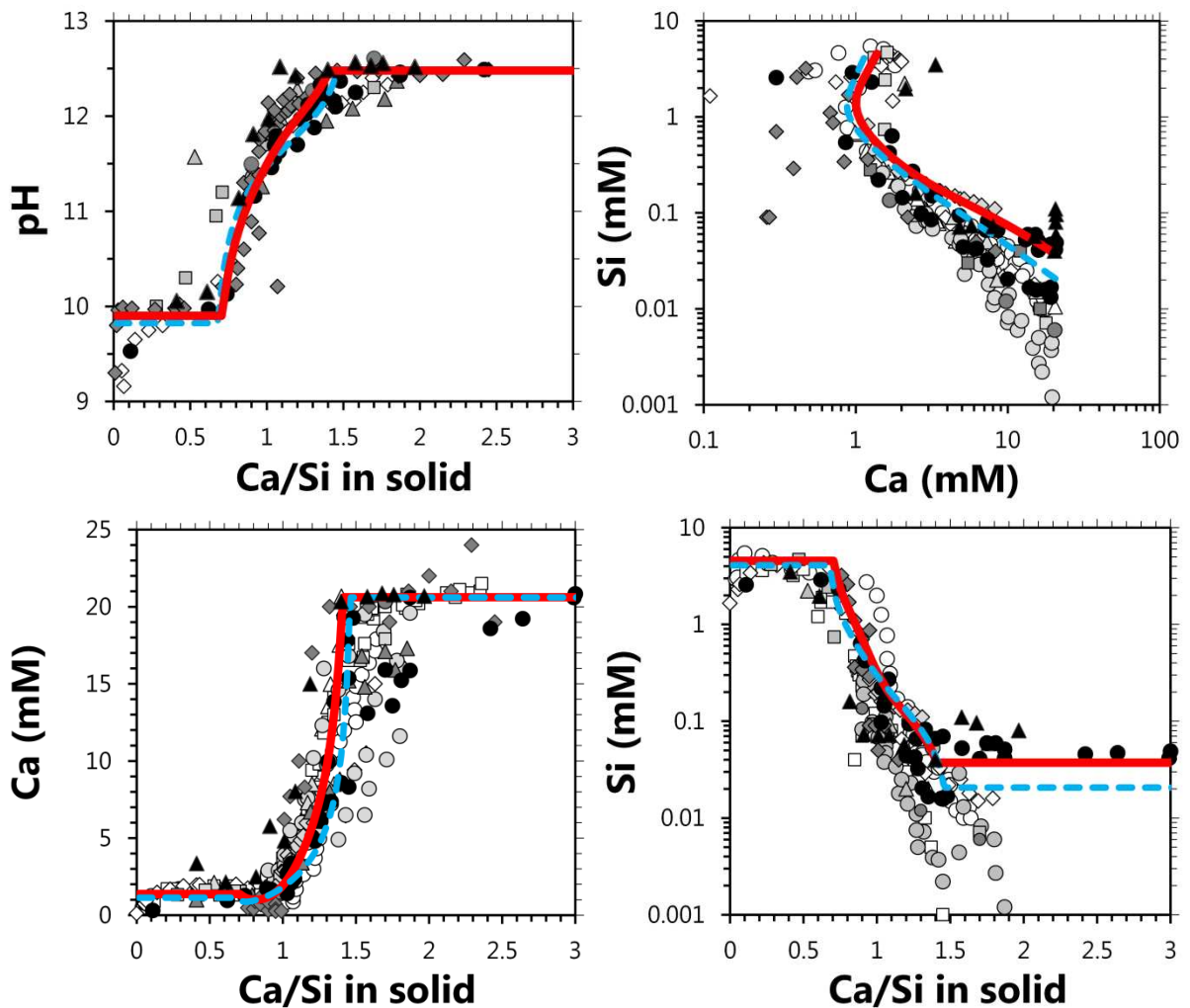
493 GEM-Selektor simulations for the $\text{CaO-SiO}_2\text{-H}_2\text{O}$ and $\text{CaO}-(\text{Na}_2\text{O},\text{Al}_2\text{O}_3)\text{-SiO}_2\text{-H}_2\text{O}$ systems were
494 performed at a constant temperature and pressure of 25°C and 1 bar, using 1 g of each of the gases
495 $\text{O}_{2(g)}$ and $\text{N}_{2(g)}$. Simulations were performed by adding H_2O , NaOH , CaO , $\text{Al}(\text{OH})_3$ and SiO_2 at a fixed
496 liquid/solid ratio = 50 using a basis of 1000 g H_2O . The C-(N-)A-S-H thermodynamic model developed
497 here (CNASH_ss) was used in all simulations. This model is provided as Electronic Supplementary
498 Information, in the correct format for use in GEM-Selektor v3. The data used for the other gases,
499 aqueous species and solid phases included in the simulations, in addition to the C-(N-)A-S-H
500 thermodynamic model developed here, are shown in Appendix C.

501

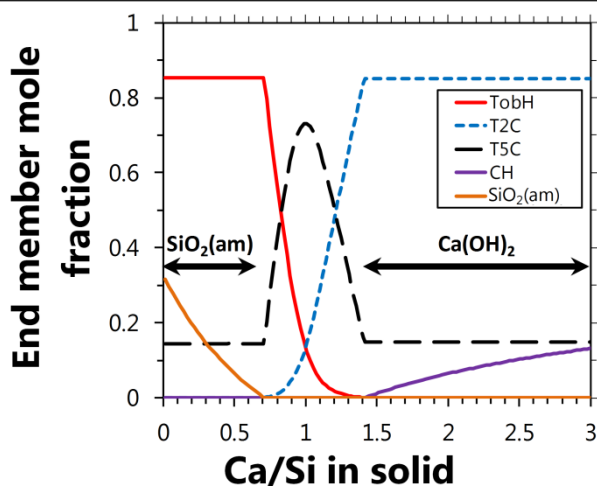
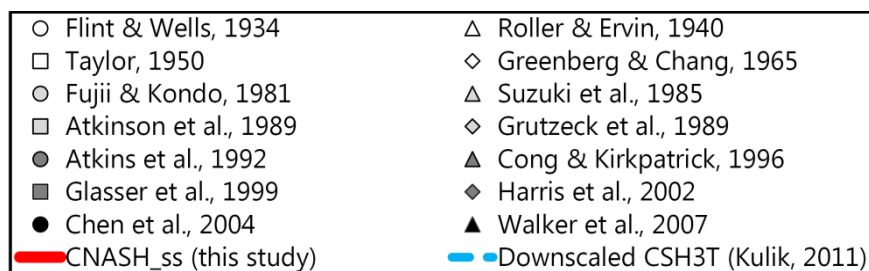
502 **6.2 Model validation in the $\text{CaO-SiO}_2\text{-H}_2\text{O}$ system**

503 An extensive body of solubility data for the $\text{CaO-SiO}_2\text{-H}_2\text{O}$ system is available [2-15], which has been
504 used to develop thermodynamic models for C-S-H gels in the past [15, 17, 18, 22, 25]. The fit of the
505 new model to these data (Figure 2) is very good regarding description of the available data for pH,
506 for concentrations of $[\text{Ca}] < 2 \text{ mmol/L (mM)}$ and $[\text{Si}] > 0.1 \text{ mM}$, and for Ca and Si solubilities up to a
507 molar Ca/Si ratio in the solid ≈ 1.3 . The thermodynamic model is less consistent with the full body of
508 available data at higher dissolved Ca concentrations, lower aqueous Si concentrations, and higher
509 Ca/Si ratios in the solid, but matches more closely with the more recently published data,
510 particularly the measurements reported in [8]. The poorer fit of the thermodynamic model to these
511 data indicate that it is partly limited by the assumption of no additional solid solution $\text{Ca}(\text{OH})_2$; the
512 simulated C-S-H gels are in equilibrium with portlandite for $\text{Ca/Si} > 1.4$ and amorphous SiO_2 is
513 simulated at Ca/Si ratios in the solid ≤ 0.67 (Figure 2). It has previously been proposed [8] that C-S-H
514 solubility varies as a function of the nanostructure of this phase, which is much more pronounced for

515 Ca/Si > 1 when many nanostructural configurations and potential bonding environments for Ca are
516 possible (for example, Ca can be accommodated in the *CB* and *IC* sites here). This would mean that
517 C-S-H thermodynamic models with a single curve for the solubility-structure relationships in these
518 gels are inherently unable to describe the full range of available solubility data for this phase.
519 However, the compositional region that is described accurately by the thermodynamic model is the
520 region of principal importance for cementitious materials with compositions in the CaO-Na₂O-Al₂O₃-
521 SiO₂-H₂O system, which typically contain C-(N-)A-S-H gels with Ca/Si ≤ 1.2 (as discussed in section 2).
522



525



526

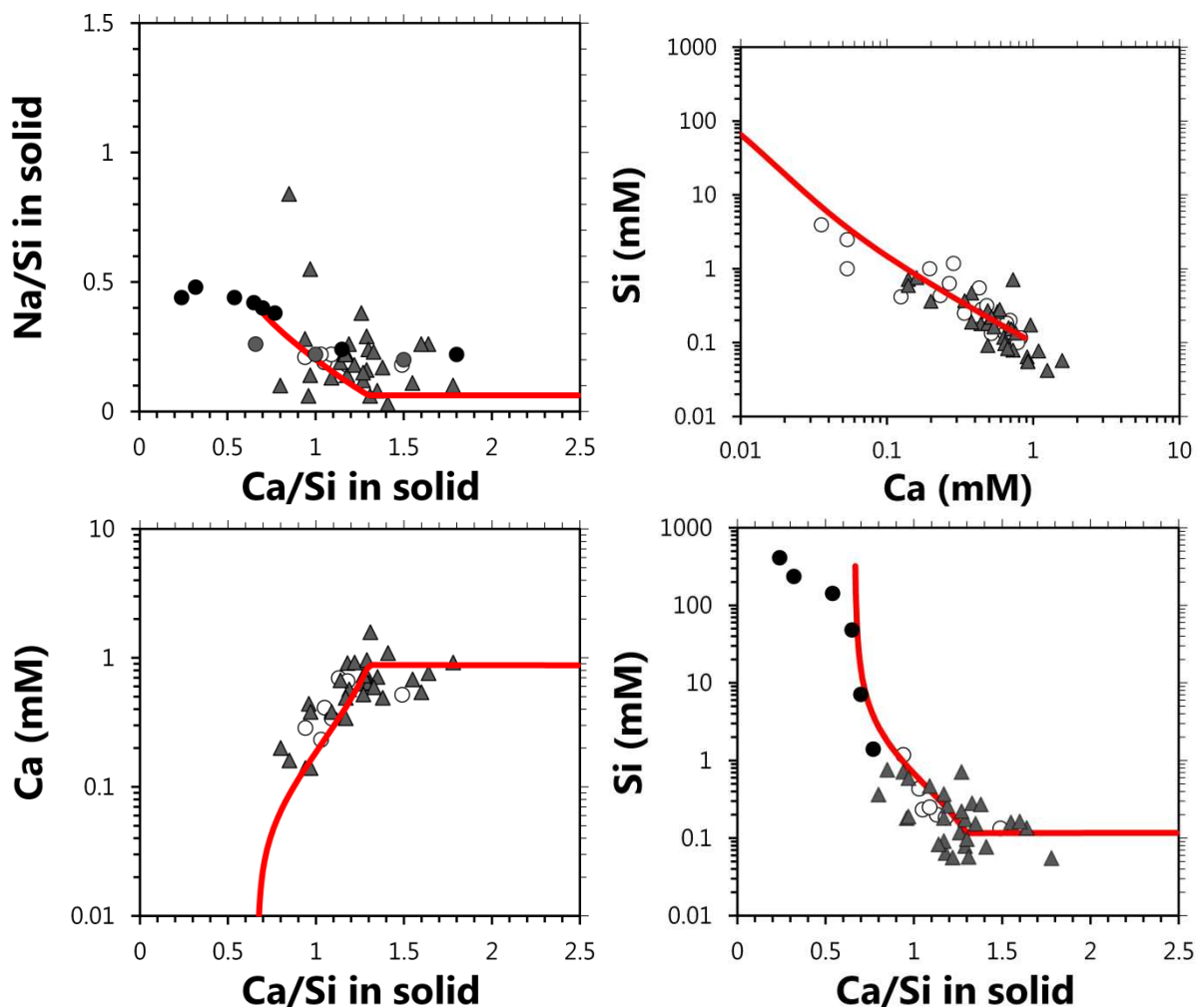
527 **Figure 2.** Comparison of the simulation results (25°C, 1 bar, water/solids mass ratio = 50) using the
 528 thermodynamic model developed here (CNASH_ss, bold red traces) to the downscaled CSH3T model
 529 (dashed blue traces) [25] and published solubility data in the CaO-SiO₂-H₂O system [2-15]. Additional
 530 plots are provided in Appendix D for the MCL and bulk chemistry results. The thermodynamic
 531 properties of the phases included in these simulations are given in Appendix C.
 532

533 6.3 Model validation in the CaO-Na₂O-SiO₂-H₂O system

534 Significantly fewer thermochemical data are available for cements in the more complex CaO-Na₂O-
 535 SiO₂-H₂O system than in the CaO-SiO₂-H₂O system. Simulations for the CaO-Na₂O-SiO₂-H₂O system
 536 (Figure 3) were performed at bulk NaOH concentrations of 0.25, 0.5, 1 and 3 mol/L, and compared to
 537 published results in the respective ranges of [NaOH] = 0.1 – 0.3 M, 0.3 – 0.8 M, 0.8 – 1 M, 1 – 5 M.
 538 This grouping was chosen to constrain the range of NaOH concentrations in the experimental studies
 539 relatively tightly to the bulk alkali concentrations used in the simulations, while maintaining enough
 540 data points in each group to enable reliable validation of the thermodynamic model. Results for the
 541 0.5 M NaOH simulation are shown in Figure 3, and the 0.25 M, 1 M and 3 M NaOH simulations are
 542 shown in Appendix D.
 543

544 The maximum Ca content of equilibrated (sodium) calcium silicate hydrate (C-(N-)S-H) gels and the
545 bulk system alkalinity are inversely related [75]; C-(N-)S-H gels with solid Ca concentrations above
546 this maximum value are more soluble than portlandite at equilibrium (a maximum value of Ca/Si \approx 1
547 has been reported for equilibrated C-(N-)S-H gels [75] at bulk NaOH concentrations \approx 1 mol/kg). The
548 thermodynamic modelling simulations performed here show this same trend (Figure 3 and Appendix
549 D), which indicate that the C-(N-)S-H gels modelled at a bulk NaOH concentration of 3 M are in
550 equilibrium with portlandite at all Ca/Si ratios \geq 1, rather than the much higher Ca/Si ratios at which
551 this is observed in the CaO-SiO₂-H₂O system (Ca/Si \geq 1.4, Figure 2).

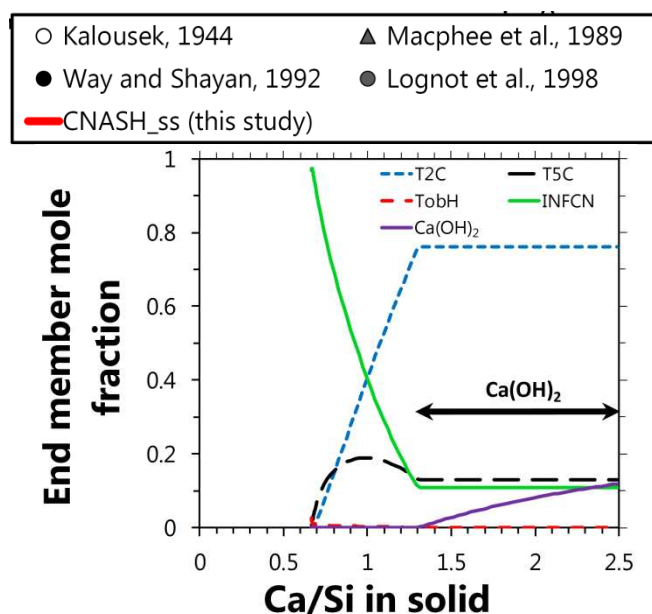
552



553

554

555



556

557 **Figure 3.** Comparison of the simulation results (25°C, 1 bar, 0.5 M NaOH/solids mass ratio = 50) using
558 the thermodynamic model developed here (CNASH_ss, bold red traces) to published solubility data
559 in the CaO-Na₂O-SiO₂-H₂O system at alkali concentrations 0.3 M ≤ [NaOH] ≤ 0.8 M [76, 77, 80, 81].
560 The simulated C-S-H gels are in equilibrium with portlandite at molar ratios of Ca/Si in the solid ≥ 1.3.
561 Additional plots are provided in Appendix D for the bulk chemistry results. The thermodynamic
562 properties of the phases included in these simulations are given in Appendix C.

563

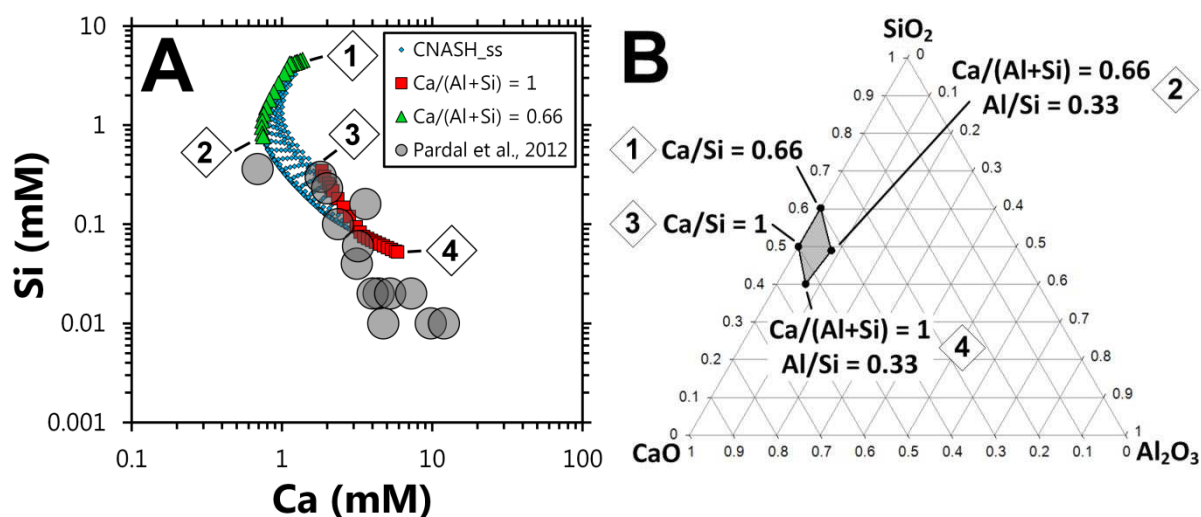
564 The good agreement between the measured solubility data for NaOH concentrations of 0.3 M-0.8 M
565 and the simulation at [NaOH] = 0.5 M is evident in Figure 3. The composition of the simulated C-(N-
566)S-H gel also captures the relatively higher Na content measured in this phase at lower Ca/Si ratios
567 [77]. The comparisons between the simulated and reported solubility data in the other alkali
568 concentration ranges studied are also good (Appendix D), with the exception of some of the data
569 reported at NaOH concentrations > 1 M in [80]. This may be explained by the presence of additional
570 sodium calcium silicate hydrate gels in those highly alkaline systems that are not described in the
571 thermodynamic databases used here (e.g. phases with similarities to the kanemite group of minerals
572 [85], which are thought to be similar to alkali-aggregate reaction products). This would mean that
573 the aqueous composition data for [NaOH] concentrations > 1 M in [80] may not be solely
574 determined by the solubility of C-(N-)S-H phases.

575

576 6.4 Model validation in the CaO-Al₂O₃-SiO₂-H₂O system

577 Analysis of C-A-S-H gel solubility from published solubility data for this phase [41, 86] is complicated
578 by the coexistence of secondary phases such as strätlingite and/or superficial carbonation products
579 (e.g. calcium hemicarboaluminate, C₄AC_{0.5}H₁₂) in the solids analysed. Here, the thermodynamic
580 model is validated against the solubility dataset published by Pardal et al. [41] (Figure 4) over the
581 bulk composition range most relevant for AAS cements, $0.66 \leq \text{Ca}/(\text{Al}+\text{Si}) \leq 1$ and $0 \leq \text{Al}/\text{Si} \leq 0.33$.
582 The simulation results and the measured solubility data are comparable, to within an order of
583 magnitude. These data show a similar inverse relationship between [Si] and [Ca] to that described by
584 the solubility data for these elements in the CaO-SiO₂-H₂O system (Figure 2).

585



586

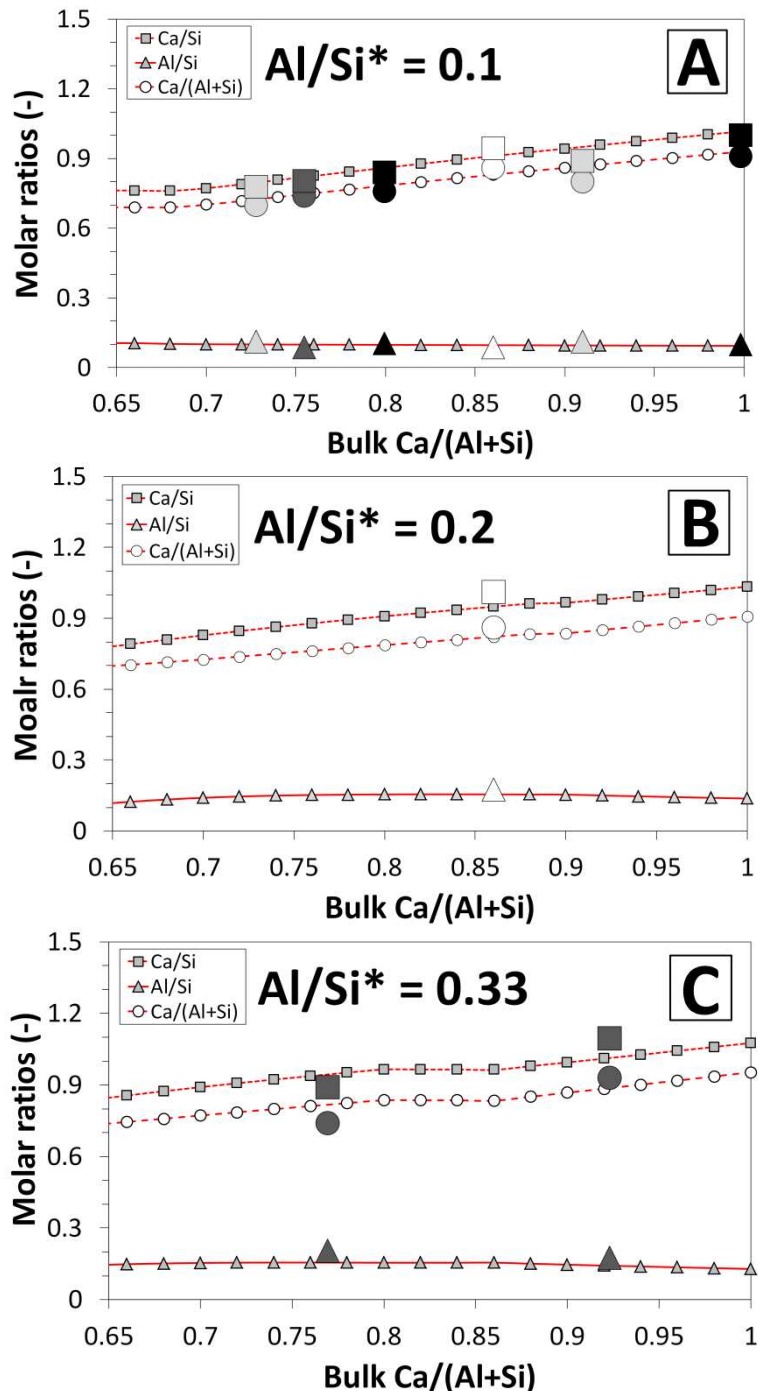
587 **Figure 4.** A) Comparison of the simulation results (25°C, 1 bar, water/solids mass ratio = 50) using the
588 thermodynamic model developed here (CNASH_{ss}, small blue diamonds, red squares and green
589 triangles) to published solubility data for C-A-S-H gels in the CaO-Al₂O₃-SiO₂-H₂O system (large grey
590 circles [41]). The corresponding range of bulk compositions simulated, projected onto the CaO-SiO₂-
591 Al₂O₃ ternary system, is shown in B). The thermodynamic properties of the phases included in these
592 simulations are given in Appendix C.

593

594 Chemical composition data for C-A-S-H gels are also used for model validation [42, 48, 78, 79]; most
595 of these data exist at three bulk Al/Si compositions: Al/Si \approx 0.1, 0.2 and 0.33. Comparison of the
596 modelling results against these data (Figures 5A-5C), for the relevant composition range in AAS

597 binders ($0.65 \leq \text{bulk Ca}/(\text{Al}+\text{Si}) \leq 1$), shows that the simulations accurately describe all of the
598 reported chemical composition data for this phase.

599



600

601

602

603 **Figure 5.** Comparison of the simulation results (25°C, 1 bar, water/solids mass ratio = 50) using the
604 thermodynamic model developed here (CNASH_ss, small symbols and red lines) to the published
605 chemical composition data for C-A-S-H gels (large symbols represent data from the literature: white
606 [42]; light grey [78]; dark grey [48]; black [79]). $\text{Al}/\text{Si}^* = \text{bulk Al}/\text{Si}$. Additional plots are provided in

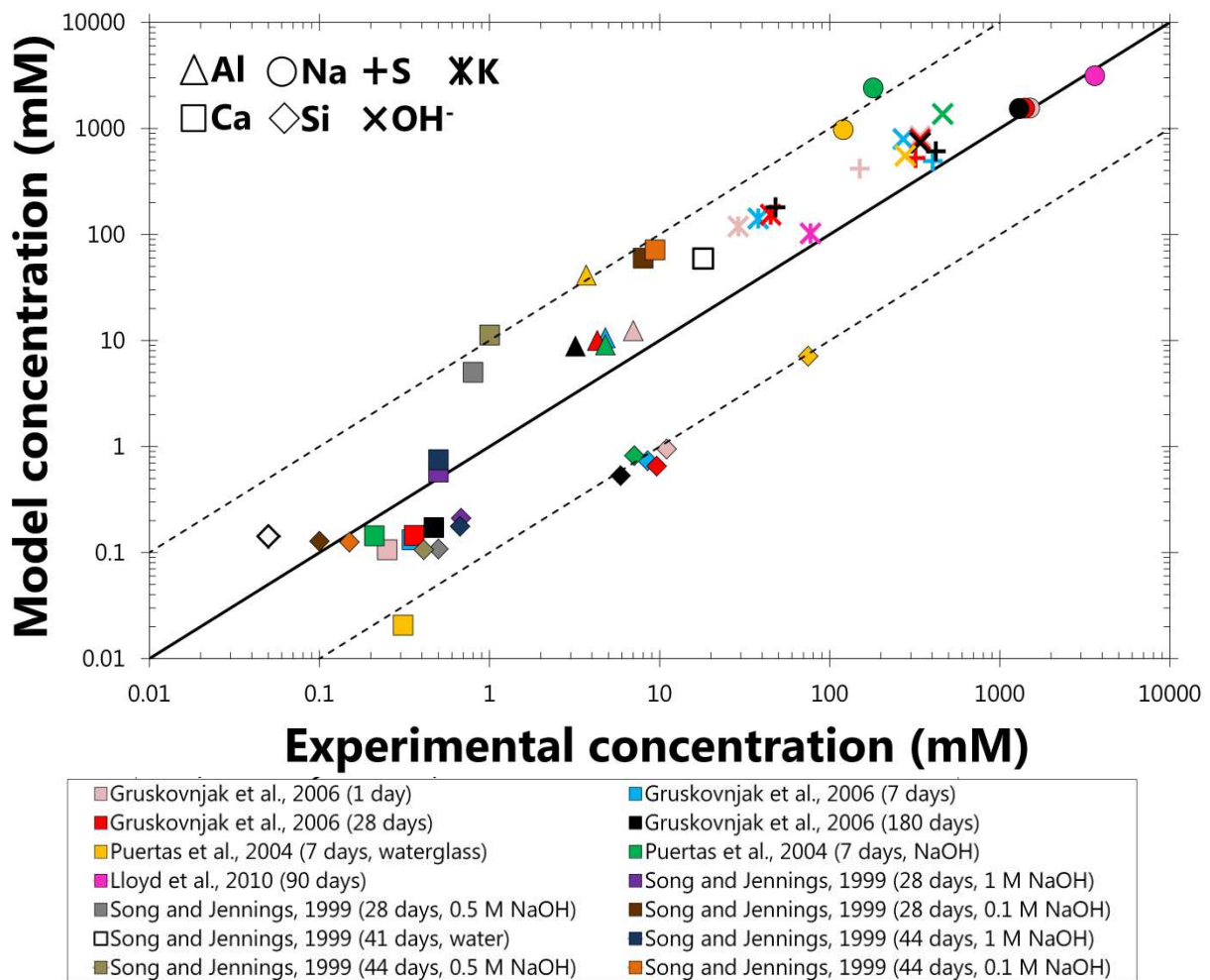
607 Appendix D for the end-member compositions. The thermodynamic properties of the phases
608 included in these simulations are given in Appendix C.
609

610 **6.5 Model validation in AAS cement systems**

611 Simulations for calculating the solubility of AAS cements were performed in an N₂ atmosphere (1 g of
612 N₂ (g), to avoid oxidation of the system) at 25°C, 1 bar and at water/binder ratios specified as
613 reported in the literature (Appendix E). Congruent slag dissolution was assumed, with the slag
614 reaction extents and bulk chemical compositions simulated by proportional additions of SiO₂, CaO,
615 MgO, Al₂O₃, Na₂O, K₂O, and H₂SO₄ or dissociated H₂S_(aq) (matching the SO₄²⁻ and S²⁻ content in the
616 slag where reported, otherwise all sulfur is assumed to be present as S²⁻), to match the bulk slag
617 chemical compositions and reaction extents reported in the literature (e.g. [45, 87, 88]). All other
618 components of the slag were excluded, as the concentrations of other elements in the slags studied
619 are minor and the reactivity of Fe entrained in slag appears to be very low [89]. For the cases where
620 the degree of reaction of the slag is needed but not available, the extent of reaction of the slag was
621 set so that the bulk chemistry of the simulations matched the bulk chemistry of the binder gel
622 assumed in the original work [50], or estimated where no further information was available (using
623 the reaction extents provided in [87] as reference values, then modifying based on the bulk alkalinity
624 and curing time).

625
626 The simulated solubility results (Figure 6) match the experimentally-measured solubility data to
627 approximately ±1 order of magnitude, with the poorest agreement found for the aqueous Si species
628 in Na₂O·*m*SiO₂·*x*H₂O-activated cements, which are under-predicted by the thermodynamic model.
629 However, the uncertainty associated with each experimental data point is expected to be large,
630 possibly also up to one order of magnitude, because slag reaction extents are not quantified in the
631 experimental studies referenced here (with the exception of the estimations in [87] for the data in
632 [71]) and the data correspond to systems that are quite far from equilibrium in some cases (e.g.
633 samples were cured for 7 days in [82]). Similar slag reaction degrees to those estimated here (~40%

634 at 100 days of curing) have been observed in sodium silicate and NaOH-activated slag pastes (35%-
 635 45% at 100 days of curing [44]), which does indicate that the estimates used here are reasonable,
 636 but does not fully resolve the uncertainty attributed to this factor. With this in mind, the accuracy of
 637 the fit between the simulation and experimental results is similar to the level of uncertainty that can
 638 be expected for modelling dissolved elemental concentrations in AAS cements.
 639



642 **Figure 6.** Simulated elemental concentrations in the aqueous phase compared to experimental pore
 643 solution composition data for AAS cements [71, 82-84]. The dotted lines show ± 1 order of
 644 magnitude deviation from the solid $y = x$ line. The thermodynamic properties of the phases included
 645 in these simulations are given in Appendix C. The slag reaction extents used in these simulations are
 646 shown in Appendix E.
 647

648 Comparisons between thermodynamic modelling results and experimental measurements of C-(N-
 649)A-S-H gel chemical compositions in AAS cements are not straightforward because secondary

650 products are often intimately intermixed with C-(N-)A-S-H gel in these materials [27] and because
 651 the nanostructure and chemical composition of this phase can vary considerably at extended ages
 652 [39]. In this sense, thermodynamic modelling can play an important role in understanding how the
 653 solid phase assemblage and chemical composition of C-(N-)A-S-H gel may change over time, with
 654 simulation results representing the predicted nature of the solid binder at equilibrium.

655
 656 It is also important to assess how accurately the thermodynamic model represents the bulk
 657 volumetric properties of C-(N-)A-S-H gels, because this is a central aspect of the application of
 658 thermodynamic modelling to cement-based materials [90]. The C-(N-)A-S-H gels formed in AAS
 659 cements are significantly denser than the C-S-H gels formed in neat PC materials [50], which is a
 660 result that should be embodied in thermodynamic models for this phase. Hence simulations using
 661 the thermodynamic model developed here are compared to the available volumetric data for C-(N-
 662)A-S-H gels in AAS cements (Table 3).

663

664 **Table 3.** Simulated C-(N-)A-S-H gel properties in AAS cements [45, 50, 88] compared to the results
 665 reported in [50], using the bulk chemistry described in that study. The thermodynamic properties of
 666 the relevant phases in these simulations are given in Appendix C.

Activator	Curing time (days)	Density (g/cm ³)	Molar volume (cm ³ /mol Si in C-(N-)A-S-H)	Reference
Experimental values				
Na ₂ O·1.82SiO ₂ ·xH ₂ O	90	2.73	50.8	[50]
Simulated values				
Na ₂ O·1.82SiO ₂ ·xH ₂ O	90	2.6	58	[50]
Na ₂ SiO ₃	180	2.7	53	COL-GBFS, [88]
Na ₂ SiO ₃	180	2.7	54	AUS-GBFS, [88]
Na ₂ SiO ₃	180	2.7	53	SP-GBFS, [88]
NaOH	100	2.6	57	[45]
Na ₂ SiO ₃ ·5H ₂ O	100	2.5	56	[45]

667

668 The C-(N-)A-S-H bulk densities and molar volumes simulated by thermodynamic modelling are
 669 similar to the reported volumetric properties of this phase (Table 3) [50]. This result is consistent
 670 with a much more tightly packed atomic structure for the C-(N-)A-S-H gels formed in AAS cements

671 than for the C-S-H gels formed in neat PC materials ((CaO)_{1.7}(SiO₂)₁(H₂O)_{1.8}, molar volume = 72.1
672 cm³/mol [91]). This is also consistent with the discussion presented in [50], where it was argued that
673 the reported density and molar volume of the C-S-H type gels formed in AAS cements are only
674 weakly related to the bulk composition of these materials. Therefore, it can be expected that the
675 thermodynamic model developed here is able to closely represent the bulk volumetric properties of
676 C-(N-)A-S-H gels in AAS cements.

677

678 **6.6 Discussion and perspectives**

679 This paper represents the first step towards developing a structurally-consistent thermodynamic
680 model for C-(N-)A-S-H gel that contains explicit descriptions of Al and alkali components, which
681 provides a relatively simple basis for further development and utilisation. Therefore, there are a
682 number of aspects that would improve the thermodynamic model, and some are listed here to guide
683 future development:

- 684 • The thermodynamic model has been designed for C-(N-)A-S-H gels with significant Al and
685 alkali incorporation, particularly those formed in AAS cement. This model may also be
686 relevant to high volume blended PC/SCM materials reacted with either water or an alkali
687 source (e.g. CEM III blast furnace cements as specified in EN 197-1), as the bulk chemical
688 compositions of these materials and AAS cements can be similar ($\text{Ca}/(\text{Al}+\text{Si}) \approx 1$) [92]. Its
689 suitability for use in simulating the chemistry of these materials needs to be assessed
690 further.
- 691 • Improvement can be found by removing the assumptions used to simplify the mixing
692 relationships for the sublattice solid solution model, which approximated the Gibbs free
693 energies of the reciprocal reactions and the excess Gibbs free energies to zero. This will
694 become possible as more information is obtained about the energetic differences arising
695 between hypothetical end-members (i.e. energetic information regarding Si-for-Al

696 substitution in chain sites, and ($\text{Ca}^{2+}, 2\text{Na}^+, 2\text{H}^+$) substitution in interlayer sites) and the
697 solubility of C-(N-)A-S-H gels.

698 • The utility of the pore solution composition data used to parameterise the thermodynamic
699 model in AAS cements would be significantly improved if such data were published
700 alongside quantification of the reaction extent of the slag. This information, along with more
701 solubility data for AAS cements and synthetic $\text{CaO-Na}_2\text{O-Al}_2\text{O}_3\text{-SiO}_2\text{-H}_2\text{O}$ systems, will be
702 needed to enable further development of thermodynamic models for C-(N-)A-S-H gels.

703

704

705 **7. Conclusions**

706

707 This paper has presented a thermodynamic model for the C-(N-)A-S-H gel in AAS cements, which for
708 the first time accounts explicitly for the structurally-incorporated Al and Na species in this phase.
709 This model represents C-(N-)A-S-H gel as an ideal solid solution of tobermorite-like end-members
710 with independent substitution of tetrahedral Al and Na species allowed in its formulation, meaning
711 that it may also be applicable to cement-based materials that are less alkali- and/or Al-rich than AAS
712 cements. The model was implemented in GEM-Selektor using thermodynamic properties for the C-
713 (N-)A-S-H end-members that were parameterised to match a comprehensive set of solubility data in
714 the $\text{CaO-(Na}_2\text{O,Al}_2\text{O}_3\text{)-SiO}_2\text{-H}_2\text{O}$ and AAS cement systems, and published chemical compositions of C-
715 A-S-H gels.

716

717 A good fit was found between the full set of data used in the parameterisation procedure and the
718 simulation results, which were within ± 1 order of magnitude in simulations of aqueous phase
719 chemical compositions in AAS cements, indicating that the model is suitable for thermodynamic
720 modelling of these materials. The molar volume and density of the C-(N-)A-S-H gels simulated by the
721 model were also in close agreement with the available data for this phase in AAS cements, meaning

722 that the model can describe chemical shrinkage in these systems. Therefore, the thermodynamic
723 model developed here greatly improves the scope of thermodynamic modelling applications to Ca-
724 rich alkali-activated cements and hybrid alkali-activated/PC materials, which is important for
725 understanding the durability of these materials under sealed, ambient and aggressive environmental
726 conditions.

727

728

729 **8. Supporting information**

730

731 The GEM-Selektor database files for the thermodynamic model developed here (CNASH_ss) are
732 provided as Electronic Supplementary Information, which can be accessed via the journal website
733 (<http://www.journals.elsevier.com/cement-and-concrete-research/>).

734

735

736 **9. Acknowledgements**

737

738 Special thanks are due to D. A. Kulik, as his contributions on thermodynamic modelling of C-S-H gels
739 provided the basis for this work [17, 25], to the team behind the freely available GEM-Selektor
740 thermodynamic modelling program (<http://gems.web.psi.ch/>) [61, 62], and to those involved in the
741 development of the thermodynamic database for cement related phases (CEMDATA) [17, 23, 64-69].

742 The authors would also like to thank the anonymous reviewers of this paper, whose comments
743 helped to substantially improve its quality and rigour.

744

745

746 **10. References**

747

- 748 [1] H.F.W. Taylor, *Cement Chemistry*, 2nd ed., Thomas Telford Publishing, London, 1997.
- 749 [2] E.P. Flint, L.S. Wells, Study of the system CaO-SiO₂-H₂O at 30°C and of the reaction of water
750 on the anhydrous calcium silicates, *J. Res. Natl. Bur. Stand.*, 12 (1934) 751-783.
- 751 [3] H.F.W. Taylor, Hydrated calcium silicates. Part I. Compound formation at ordinary
752 temperatures, *J. Chem. Soc.*, (1950) 3682-3690.
- 753 [4] K. Fujii, W. Kondo, Heterogeneous equilibrium of calcium silicate hydrate in water at 30°C, *J.*
754 *Chem. Soc., Dalton Trans.*, (1981) 645-651.
- 755 [5] A. Atkinson, J.A. Hearne, C.F. Knights, Aqueous chemistry and thermodynamic modelling of
756 CaO-SiO₂-H₂O gels, *J. Chem. Soc., Dalton Trans.*, (1989) 2371-2379.
- 757 [6] M. Atkins, F.P. Glasser, A. Kindness, Cement hydrate phase: solubility at 25°C, *Cem. Concr.*
758 *Res.*, 22 (1992) 241-246.
- 759 [7] F.P. Glasser, M. Tyrer, K. Quillin, D. Ross, J. Pedersen, K. Goldthorpe, D. Bennett, M. Atkins,
760 The chemistry of blended cements and backfills intended for use in radioactive waste
761 disposal: R&D technical report P98, Bristol, 1999.
- 762 [8] J.J. Chen, J.J. Thomas, H.F.W. Taylor, H.M. Jennings, Solubility and structure of calcium
763 silicate hydrate, *Cem. Concr. Res.*, 34 (2004) 1499-1519.
- 764 [9] P.S. Roller, G. Ervin, The system calcium oxide-silica-water at 30°C. The association of silicate
765 ion in dilute alkaline solution, *J. Am. Chem. Soc.*, 62 (1940) 461-471.
- 766 [10] S.A. Greenberg, T.N. Chang, Investigation of the colloidal hydrated calcium silicates. II.
767 Solubility relationships in the calcium oxide-silica-water system at 25°C, *J. Phys. Chem.*, 69
768 (1965) 182-188.
- 769 [11] K. Suzuki, T. Nishikawa, S. Ito, Formation and carbonation of C-S-H in water, *Cem. Concr.*
770 *Res.*, 15 (1985) 213-224.
- 771 [12] M. Grutzeck, A. Benesi, B. Fanning, Silicon-29 magic angle spinning nuclear magnetic
772 resonance study of calcium silicate hydrates, *J. Am. Ceram. Soc.*, 72 (1989) 665-668.
- 773 [13] X. Cong, R.J. Kirkpatrick, ²⁹Si MAS NMR study of the structure of calcium silicate hydrate,
774 *Adv. Cem. Based Mater.*, 3 (1996) 144-156.
- 775 [14] A.W. Harris, M.C. Manning, W.M. Tearle, C.J. Tweed, Testing of models of the dissolution of
776 cements—leaching of synthetic CSH gels, *Cem. Concr. Res.*, 32 (2002) 731-746.
- 777 [15] C.S. Walker, D. Savage, M. Tyrer, K.V. Ragnarsdottir, Non-ideal solid solution aqueous
778 solution modeling of synthetic calcium silicate hydrate, *Cem. Concr. Res.*, 37 (2007) 502-511.
- 779 [16] H.M. Jennings, Aqueous solubility relationships for two types of calcium silicate hydrate, *J.*
780 *Am. Ceram. Soc.*, 69 (1986) 614-618.

- 781 [17] D.A. Kulik, M. Kersten, Aqueous solubility diagrams for cementitious waste stabilization
782 systems: II. End-member stoichiometries of ideal calcium silicate hydrate solid solutions, *J.*
783 *Am. Ceram. Soc.*, 84 (2001) 3017-3026.
- 784 [18] U.R. Berner, Evolution of pore water chemistry during degradation of cement in a
785 radioactive waste repository environment, *Waste Manage.*, 12 (1992) 201-219.
- 786 [19] F.P. Glasser, E.E. Lachowski, D.E. Macphee, Compositional model for calcium silicate hydrate
787 (C-S-H) gels, their solubilities, and free energies of formation, *J. Am. Ceram. Soc.*, 70 (1987)
788 481-485.
- 789 [20] E.J. Reardon, An ion interaction model for the determination of chemical equilibria in
790 cement/water systems, *Cem. Concr. Res.*, 20 (1990) 175-192.
- 791 [21] M. Atkins, D.G. Bennett, A.C. Dawes, F.P. Glasser, A. Kindness, D. Read, A thermodynamic
792 model for blended cements, *Cem. Concr. Res.*, 22 (1992) 497-502.
- 793 [22] J.A. Gisby, R.H. Davies, A.T. Dinsdale, M. Tyrer, F.P. Glasser, J. Hill, P. Livesey, C. Walker, C-S-
794 H solubility modeling at different temperatures, in: *Proceedings of the 12th International*
795 *Congress on the Chemistry of Cement*, Cement Association of Canada, Montreal, 2007.
- 796 [23] B. Lothenbach, F. Winnefeld, Thermodynamic modelling of the hydration of Portland
797 cement, *Cem. Concr. Res.*, 36 (2006) 209-226.
- 798 [24] B. Lothenbach, Thermodynamic equilibrium calculations in cementitious systems, *Mater.*
799 *Struct.*, 43 (2010) 1413-1433.
- 800 [25] D.A. Kulik, Improving the structural consistency of C-S-H solid solution thermodynamic
801 models, *Cem. Concr. Res.*, 41 (2011) 477-495.
- 802 [26] B. Lothenbach, K. Scrivener, R.D. Hooton, Supplementary cementitious materials, *Cem.*
803 *Concr. Res.*, 41 (2011) 1244-1256.
- 804 [27] I.G. Richardson, G.W. Groves, Microstructure and microanalysis of hardened cement pastes
805 involving ground granulated blast-furnace slag, *J. Mater. Sci.*, 27 (1992) 6204-6212.
- 806 [28] J.L. Provis, S.A. Bernal, Geopolymers and related alkali-activated materials, *Annu. Rev.*
807 *Mater. Res.*, 44 (2014) 3.1-3.29.
- 808 [29] C. Shi, P.V. Krivenko, D. Roy, *Alkali-Activated Cements and Concretes*, 1st ed., Taylor &
809 Francis, New York, 2006.
- 810 [30] M. Atkins, F. Glasser, L.P. Moroni, J.J. Jack, Thermodynamic modelling of blended cements at
811 elevated temperature (50-90°C), Aberdeen University, United Kingdom,
812 DoE1HMIP1RR/94.011, 1994.
- 813 [31] M. Ben Haha, B. Lothenbach, G. Le Saoût, F. Winnefeld, Influence of slag chemistry on the
814 hydration of alkali-activated blast-furnace slag - part II: effect of Al₂O₃, *Cem. Concr. Res.*, 42
815 (2012) 74-83.
- 816 [32] W. Loewenstein, The distribution of aluminum in the tetrahedra of silicates and aluminates,
817 *Am. Mineral.*, 39 (1954) 92-96.

- 818 [33] L. Pegado, C. Labbez, S.V. Churakov, Mechanism of aluminium incorporation into C-S-H from
819 ab initio calculations, *J. Mater. Chem. A*, 2 (2014) 3477-3483.
- 820 [34] I.G. Richardson, A.R. Brough, R. Brydson, G.W. Groves, C.M. Dobson, Location of aluminum
821 in substituted calcium silicate hydrate (C-S-H) gels as determined by ^{29}Si and ^{27}Al NMR and
822 EELS, *J. Am. Ceram. Soc.*, 76 (1993) 2285-2288.
- 823 [35] I.G. Richardson, A.R. Brough, G.W. Groves, C.M. Dobson, The characterization of hardened
824 alkali-activated blast-furnace slag pastes and the nature of the calcium silicate hydrate (C-S-
825 H) phase, *Cem. Concr. Res.*, 24 (1994) 813-829.
- 826 [36] F. Puertas, M. Palacios, H. Manzano, J.S. Dolado, A. Rico, J. Rodríguez, A model for the C-A-S-
827 H gel formed in alkali-activated slag cements, *J. Eur. Ceram. Soc.*, 31 (2011) 2043-2056.
- 828 [37] F. Bonk, J. Schneider, M.A. Cincotto, H. Panepucci, Characterization by multinuclear high-
829 resolution NMR of hydration products in activated blast-furnace slag pastes, *J. Am. Ceram.*
830 *Soc.*, 86 (2003) 1712-1719.
- 831 [38] I.G. Richardson, G.W. Groves, The incorporation of minor and trace elements into calcium
832 silicate hydrate (C-S-H) gel in hardened cement pastes, *Cem. Concr. Res.*, 23 (1993) 131-138.
- 833 [39] R.J. Myers, S.A. Bernal, R. San Nicolas, J.L. Provis, Generalized structural description of
834 calcium-sodium aluminosilicate hydrate gels: the cross-linked substituted tobermorite
835 model, *Langmuir*, 29 (2013) 5294-5306.
- 836 [40] A. Fernández-Jiménez, F. Puertas, I. Sobrados, J. Sanz, Structure of calcium silicate hydrates
837 formed in alkaline-activated slag: Influence of the type of alkaline activator, *J. Am. Ceram.*
838 *Soc.*, 86 (2003) 1389-1394.
- 839 [41] X. Pardal, F. Brunet, T. Charpentier, I. Pochard, A. Nonat, ^{27}Al and ^{29}Si solid-state NMR
840 characterization of calcium-aluminosilicate-hydrate, *Inorg. Chem.*, 51 (2012) 1827-1836.
- 841 [42] G.K. Sun, J.F. Young, R.J. Kirkpatrick, The role of Al in C-S-H: NMR, XRD, and compositional
842 results for precipitated samples, *Cem. Concr. Res.*, 36 (2006) 18-29.
- 843 [43] S.D. Wang, K.L. Scrivener, Hydration products of alkali activated slag cement, *Cem. Concr.*
844 *Res.*, 25 (1995) 561-571.
- 845 [44] M. Ben Haha, G. Le Saoût, F. Winnefeld, B. Lothenbach, Influence of activator type on
846 hydration kinetics, hydrate assemblage and microstructural development of alkali activated
847 blast-furnace slags, *Cem. Concr. Res.*, 41 (2011) 301-310.
- 848 [45] G. Le Saoût, M. Ben Haha, F. Winnefeld, B. Lothenbach, Hydration degree of alkali-activated
849 slags: a ^{29}Si NMR study, *J. Am. Ceram. Soc.*, 94 (2011) 4541-4547.
- 850 [46] A.R. Brough, A. Atkinson, Sodium silicate-based, alkali-activated slag mortars - Part I.
851 Strength, hydration and microstructure, *Cem. Concr. Res.*, 32 (2002) 865-879.
- 852 [47] X. Pardal, I. Pochard, A. Nonat, Experimental study of Si-Al substitution in calcium-silicate-
853 hydrate (C-S-H) prepared under equilibrium conditions, *Cem. Concr. Res.*, 39 (2009) 637-643.

- 854 [48] P. Faucon, A. Delagrave, J.C. Petit, C. Richet, J.M. Marchand, H. Zanni, Aluminum
855 incorporation in calcium silicate hydrates (C-S-H) depending on their Ca/Si ratio, *J. Phys.*
856 *Chem. B*, 103 (1999) 7796-7802.
- 857 [49] H.M. Jennings, Refinements to colloid model of C-S-H in cement: CM-II, *Cem. Concr. Res.*, 38
858 (2008) 275-289.
- 859 [50] J.J. Thomas, A.J. Allen, H.M. Jennings, Density and water content of nanoscale solid C-S-H
860 formed in alkali-activated slag (AAS) paste and implications for chemical shrinkage, *Cem.*
861 *Concr. Res.*, 42 (2012) 377-383.
- 862 [51] E. Bonaccorsi, S. Merlino, A.R. Kampf, The crystal structure of tobermorite 14Å (plombierite),
863 a C-S-H phase, *J. Am. Ceram. Soc.*, 88 (2005) 505-512.
- 864 [52] S. Merlino, E. Bonaccorsi, T. Armbruster, The real structure of tobermorite 11Å: normal and
865 anomalous forms, OD character and polytypic modifications, *Eur. J. Mineral.*, 13 (2001) 577-
866 590.
- 867 [53] I.G. Richardson, Tobermorite/jennite- and tobermorite/calcium hydroxide-based models for
868 the structure of C-S-H: applicability to hardened pastes of tricalcium silicate, β -dicalcium
869 silicate, Portland cement, and blends of Portland cement with blast-furnace slag,
870 metakaolin, or silica fume, *Cem. Concr. Res.*, 34 (2004) 1733-1777.
- 871 [54] I.G. Richardson, The calcium silicate hydrates, *Cem. Concr. Res.*, 38 (2008) 137-158.
- 872 [55] I.G. Richardson, G.W. Groves, Models for the composition and structure of calcium silicate
873 hydrate (CSH) gel in hardened tricalcium silicate pastes, *Cem. Concr. Res.*, 22 (1992) 1001-
874 1010.
- 875 [56] A.J. Allen, J.J. Thomas, H.M. Jennings, Composition and density of nanoscale calcium-silicate-
876 hydrate in cement, *Nat. Mater.*, 6 (2007) 311-316.
- 877 [57] M. Hillert, Phase equilibria, phase diagrams and phase transformations: their
878 thermodynamic basis, Cambridge University Press, Cambridge, 1998.
- 879 [58] M. Hillert, L.-I. Staffansson, The regular solution model for stoichiometric phases and ionic
880 melts, *Acta Chem. Scand.*, 24 (1970) 3618-3626.
- 881 [59] J.O. Andersson, A.F. Guillermet, M. Hillert, B. Jansson, B. Sundman, A compound-energy
882 model of ordering in a phase with sites of different coordination numbers, *Acta Metall.*
883 *Mater.*, 34 (1986) 437-445.
- 884 [60] J.L. Provis, P. Duxson, G.C. Lukey, J.S.J. Van Deventer, Statistical thermodynamic model for
885 Si/Al ordering in amorphous aluminosilicates, *Chem. Mater.*, 17 (2005) 2976-2986.
- 886 [61] D.A. Kulik, T. Wagner, S.V. Dmytrieva, G. Kosakowski, F.F. Hingerl, K.V. Chudnenko, U.
887 Berner, GEM-Selektor geochemical modeling package: revised algorithm and GEMS3K
888 numerical kernel for coupled simulation codes, *Comput. Geosci.*, 17 (2013) 1-24.
- 889 [62] T. Wagner, D.A. Kulik, F.F. Hingerl, S.V. Dmytrieva, GEM-Selektor geochemical modeling
890 package: TSolMod library and data interface for multicomponent phase models, *Can.*
891 *Mineral.*, 50 (2012) 1173-1195.

- 892 [63] W. Hummel, U. Berner, E. Curti, F.J. Pearson, T. Thoenen, Nagra/PSI Chemical
893 Thermodynamic Database 01/01, Universal Publishers, Parkland, 2002.
- 894 [64] T. Matschei, B. Lothenbach, F.P. Glasser, Thermodynamic properties of Portland cement
895 hydrates in the system CaO-Al₂O₃-SiO₂-CaSO₄-CaCO₃-H₂O, *Cem. Concr. Res.*, 37 (2007) 1379-
896 1410.
- 897 [65] T. Schmidt, B. Lothenbach, M. Romer, K. Scrivener, D. Rentsch, R. Figi, A thermodynamic and
898 experimental study of the conditions of thaumasite formation, *Cem. Concr. Res.*, 38 (2008)
899 337-349.
- 900 [66] B. Lothenbach, T. Matschei, G. Möschner, F.P. Glasser, Thermodynamic modelling of the
901 effect of temperature on the hydration and porosity of Portland cement, *Cem. Concr. Res.*,
902 38 (2008) 1-18.
- 903 [67] D.A. Kulik, M. Kersten, Aqueous solubility diagrams for cementitious waste stabilization
904 systems. 4. A carbonation model for Zn-doped calcium silicate hydrate by Gibbs energy
905 minimization, *Environ. Sci. Technol.*, 36 (2002) 2926-2931.
- 906 [68] G. Möschner, B. Lothenbach, J. Rose, A. Ulrich, R. Figi, R. Kretzschmar, Solubility of Fe-
907 ettringite (Ca₆[Fe(OH)₆]₂(SO₄)₃·26H₂O), *Geochim. Cosmochim. Acta*, 72 (2008) 1-18.
- 908 [69] G. Möschner, B. Lothenbach, F. Winnefeld, A. Ulrich, R. Figi, R. Kretzschmar, Solid solution
909 between Al-ettringite and Fe-ettringite (Ca₆[Al_{1-x}Fe_x(OH)₆]₂(SO₄)₃·26H₂O), *Cem. Concr. Res.*,
910 39 (2009) 482-489.
- 911 [70] H.C. Helgeson, D.H. Kirkham, G.C. Flowers, Theoretical prediction of the thermodynamic
912 behavior of aqueous electrolytes at high pressures and temperatures: IV. Calculation of
913 activity coefficients, osmotic coefficients, and apparent molal and standard and relative
914 partial molal properties to 600°C and 5 kb, *Am. J. Sci.*, 281 (1981) 1249-1516.
- 915 [71] A. Gruskovnjak, B. Lothenbach, L. Holzer, R. Figi, F. Winnefeld, Hydration of alkali-activated
916 slag: Comparison with ordinary Portland cement, *Adv. Cem. Res.*, 18 (2006) 119-128.
- 917 [72] K.S. Pitzer, Ion interaction approach: theory and data correlation, in: *Activity Coefficients in*
918 *Electrolyte Solutions*, CRC Press, Boca Raton, 1991, 75-153.
- 919 [73] J.L. Provis, P. Duxson, G.C. Lukey, F. Separovic, W.M. Kriven, J.S.J. Van Deventer, Modeling
920 speciation in highly concentrated alkaline silicate solutions, *Ind. Eng. Chem. Res.*, 44 (2005)
921 8899-8908.
- 922 [74] G.M. Anderson, D.A. Crerar, *Thermodynamics in geochemistry: the equilibrium model*,
923 Oxford University Press, Oxford, 1993.
- 924 [75] I. Lognot, I. Klur, A. Nonat, NMR and infrared spectroscopies of C-S-H and Al-substituted C-S-
925 H synthesised in alkaline solutions, in: P. Colombet, H. Zanni, A.-R. Grimmer, P. Sozzani (Eds.)
926 *Nuclear magnetic resonance spectroscopy of cement-based materials*, Springer Berlin
927 Heidelberg, 1998, 189-196.
- 928 [76] S.Y. Hong, F.P. Glasser, Alkali binding in cement pastes: part I. The C-S-H phase, *Cem. Concr.*
929 *Res.*, 29 (1999) 1893-1903.

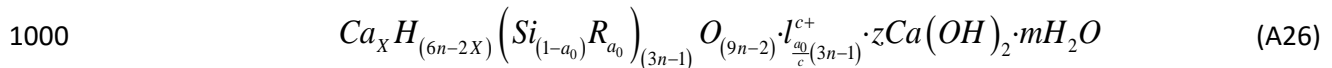
- 930 [77] S.J. Way, A. Shayan, Study of some synthetically prepared hydrous alkali calcium silicates,
931 *Cem. Concr. Res.*, 22 (1992) 915-926.
- 932 [78] G. Renaudin, J. Russias, F. Leroux, F. Frizon, C. Cau-dit-Coumes, Structural characterization of
933 C-S-H and C-A-S-H samples - part I: long-range order investigated by Rietveld analyses, *J.*
934 *Solid State Chem.*, 182 (2009) 3312-3319.
- 935 [79] G. Renaudin, J. Russias, F. Leroux, C. Cau-dit-Coumes, F. Frizon, Structural characterization of
936 C-S-H and C-A-S-H samples - part II: local environment investigated by spectroscopic
937 analyses, *J. Solid State Chem.*, 182 (2009) 3320-3329.
- 938 [80] G.L. Kalousek, Studies of portions of the quaternary system soda-lime-silica-water at 25°C, *J.*
939 *Res. Natl. Bur. Stand.*, 32 (1944) 285-302.
- 940 [81] D.E. Macphee, K. Luke, F.P. Glasser, E.E. Lachowski, Solubility and aging of calcium silicate
941 hydrates in alkaline solutions at 25°C, *J. Am. Ceram. Soc.*, 72 (1989) 646-654.
- 942 [82] F. Puertas, A. Fernández-Jiménez, M.T. Blanco-Varela, Pore solution in alkali-activated slag
943 cement pastes. Relation to the composition and structure of calcium silicate hydrate, *Cem.*
944 *Concr. Res.*, 34 (2004) 139-148.
- 945 [83] R.R. Lloyd, J.L. Provis, J.S.J. van Deventer, Pore solution composition and alkali diffusion in
946 inorganic polymer cement, *Cem. Concr. Res.*, 40 (2010) 1386-1392.
- 947 [84] S. Song, H.M. Jennings, Pore solution chemistry of alkali-activated ground granulated blast-
948 furnace slag, *Cem. Concr. Res.*, 29 (1999) 159-170.
- 949 [85] R.J. Kirkpatrick, A.G. Kalinichev, X. Hou, L. Struble, Experimental and molecular dynamics
950 modeling studies of interlayer swelling: water incorporation in kanemite and ASR gel, *Mater.*
951 *Struct.*, 38 (2005) 449-458.
- 952 [86] P. Faucon, J.C. Petit, T. Charpentier, J.F. Jacquinet, F. Adenot, Silicon Substitution for
953 Aluminum in Calcium Silicate Hydrates, *J. Am. Ceram. Soc.*, 82 (1999) 1307-1312.
- 954 [87] B. Lothenbach, A. Gruskovnjak, Hydration of alkali-activated slag: thermodynamic modelling,
955 *Adv. Cem. Res.*, 19 (2007) 81-92.
- 956 [88] S.A. Bernal, R. San Nicolas, R.J. Myers, R. Mejía de Gutiérrez, F. Puertas, J.S.J. van Deventer,
957 J.L. Provis, MgO content of slag controls phase evolution and structural changes induced by
958 accelerated carbonation in alkali-activated binders, *Cem. Concr. Res.*, 57 (2014) 33-43.
- 959 [89] S.A. Bernal, V. Rose, J.L. Provis, The fate of iron in blast furnace slag particles during alkali-
960 activation, *Mater. Chem. Phys.*, 146 (2014) 1-5.
- 961 [90] B. Lothenbach, G. Le Saout, E. Gallucci, K. Scrivener, Influence of limestone on the hydration
962 of Portland cements, *Cem. Concr. Res.*, 38 (2008) 848-860.
- 963 [91] A.J. Allen, J.J. Thomas, Analysis of C-S-H gel and cement paste by small-angle neutron
964 scattering, *Cem. Concr. Res.*, 37 (2007) 319-324.
- 965 [92] R. Taylor, I.G. Richardson, R.M.D. Brydson, Composition and microstructure of 20-year-old
966 ordinary Portland cement-ground granulated blast-furnace slag blends containing 0 to 100%
967 slag, *Cem. Concr. Res.*, 40 (2010) 971-983.

- 968 [93] R.A. Robie, B.S. Hemingway, Thermodynamic properties of minerals and related substances
969 at 298.15 K and 1 bar (10^5 Pascals) pressure and at higher temperatures, United States
970 Government Printing Office, Washington D.C., 1995.
- 971 [94] H.C. Helgeson, J.M. Delany, H.W. Nesbitt, Summary and critique of the thermodynamic
972 properties of rock-forming minerals, *Am. J. Sci.*, 278-A (1978).
- 973 [95] M.W. Chase, Jr., NIST-JANAF Thermochemical Tables, Fourth Edition, *J. Phys. Chem. Ref.*
974 *Data*, 4th Ed., 1998.
- 975 [96] D.D. Wagman, W.H. Evans, V.B. Parker, R.H. Schumm, I. Halow, The NBS tables of chemical
976 thermodynamic properties: selected values for inorganic and C₁ and C₂ organic substances in
977 SI units, American Chemical Society and the American Institute of Physics for the National
978 Bureau of Standards, New York, 1982.
- 979 [97] E.L. Shock, D.C. Sassani, M. Willis, D.A. Sverjensky, Inorganic species in geologic fluids:
980 correlations among standard molal thermodynamic properties of aqueous ions and
981 hydroxide complexes, *Geochim. Cosmochim. Acta*, 61 (1997) 907-950.
- 982 [98] D.A. Sverjensky, E.L. Shock, H.C. Helgeson, Prediction of the thermodynamic properties of
983 aqueous metal complexes to 1000°C and 5 kb, *Geochim. Cosmochim. Acta*, 61 (1997) 1359-
984 1412.
- 985 [99] E.L. Shock, H.C. Helgeson, D.A. Sverjensky, Calculation of the thermodynamic and transport
986 properties of aqueous species at high pressures and temperatures: standard partial molal
987 properties of inorganic neutral species, *Geochim. Cosmochim. Acta*, 53 (1989) 2157-2183.
- 988 [100] J.W. Johnson, E.H. Oelkers, H.C. Helgeson, SUPCRT92: A software package for calculating the
989 standard molal thermodynamic properties of minerals, gases, aqueous species, and
990 reactions from 1 to 5000 bar and 0 to 1000°C, *Comput. Geosci.*, 18 (1992) 899-947.
- 991 [101] B. Lothenbach, L. Pelletier-Chaignat, F. Winnefeld, Stability in the system CaO–Al₂O₃–H₂O,
992 *Cem. Concr. Res.*, 42 (2012) 1621-1634.
- 993
- 994

995 **Appendix A. Additional details of the C-(N-)A-S-H sublattice solid**
 996 **solution model**

997

998 Derivation of the C-(N-)A-S-H thermodynamic model begins by rearranging the SGM (eq.(A1), [38])
 999 into an alternative structural form:

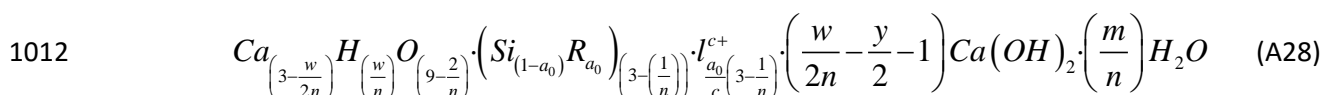


1001 where R is a trivalent cation in tetrahedral coordination (e.g. Al^{3+}), l is a charge-balancing interlayer
 1002 cation (such as Ca^{2+}) with a positive charge of c , m defines the amount of bound interlayer water, n is
 1003 the number of dreierketten units per non-crosslinked C-(N-)A-S-H chain, a_0 is the extent of
 1004 substitution in aluminosilicate chains and the parameters X , z , a_0 and n are defined according to
 1005 eq.(A2):

1006
$$\left. \begin{aligned} X &= 0.5(6n - w) \\ z &= 0.5[w + n(y - 2)] \\ 0 \leq a_0 &\leq \frac{n-1}{(3n-1)} \end{aligned} \right\} \quad (A27)$$

1007

1008 The parameters w and y are related to the extent of protonation of chain tetrahedra and amount of
 1009 solid solution $Ca(OH)_2$ present in the gel. Rearrangement of the SGM begins by normalising eq.(A1)
 1010 to a basis of one dreierketten unit by dividing by n , expressed in terms of w and n for X and z , and
 1011 then simplified to obtain eq.(A3):



1013

1014 The following notation is now introduced into eq.(A3): $v = 1/n$ ($0 \leq v \leq 1$), defines the ratio of chains
 1015 per dreierketten unit, which is a measure of the number of vacant bridging tetrahedra; $u = w/n$, the

1016 content of chemically incorporated (hydroxyl) water per dreierketten unit; and $h = m/n$, the bound
 1017 water content. The introduction of this notation results in eq.(A4):

$$1018 \quad Ca_{\left(3-\frac{u}{2}\right)} H_u O_{(9-2\nu)} \cdot \left(Si_{(1-a_0)} R_{a_0} \right)_{(3-\nu)} \cdot I_{\frac{a_0}{\nu}(3-\nu)}^{c+} \cdot \left(\frac{u}{2} - \frac{y}{2} - 1 \right) Ca(OH)_2 \cdot hH_2O \quad (A29)$$

1019

1020 Eq.(A4) is then re-written to isolate two distinct sublattice sites within the chain structure, being a
 1021 ‘main chain dreierketten unit’ (*TU*) and a ‘bridging tetrahedral unit’ (*BT*). This leads to a subtle
 1022 change in the substitution parameter, a_0 , which is now written as a , the extent of substitution in
 1023 bridging sites. The resulting equation is:

$$1024 \quad \left[Ca(OH)_2 \right]_{\left(\frac{u+y-2}{2}\right)} \cdot \left[(CaSiO_{3.5})_2 \right] \cdot \left[\left(Si_{(1-a)} R_a O_2 \right)_{(1-\nu)} \right]^{a(1-\nu)-} \cdot \left[\left(I_{\frac{a}{\nu}(1-\nu)}^{c+} \right) \right]^{a(1-\nu)+} \cdot \left[Ca_{\left(1-\frac{u}{2}\right)} H_u \right]^{2+} \cdot hH_2O \quad (A30)$$

1025

1026 Eq.(A5) is equivalent to eq.(2) in the main body of the text.

1027

1028 **Appendix B. Activity coefficient relationships for the C-(N-)A-S-H end-**
 1029 **members**

1030

1031 The relationships for the fictive activity coefficients for the end-members of the C-(N-)A-S-H
 1032 sublattice solid solution model are defined here in terms of the following notation: 5CA = 0, INFCA =
 1033 1, 5CNA = 2, INFCNA = 3, INFCN = 4, T2C* = 5, T5C* = 6, TobH* = 7.

1034

1035
$$\ln(\lambda_0) = 2\ln(\chi_0 + \chi_1) + 2\ln(\chi_0 + \chi_1) + 2\ln(\chi_0 + \chi_2 + \chi_5 + \chi_6) +$$

$$\ln(\chi_0 + \chi_5 + \chi_6) + \ln(\chi_0 + \chi_5 + \chi_6) + \ln(\chi_0 + \chi_1 + \chi_2 + \chi_3 + \chi_4) - \ln(\chi_0)$$
 (B31)

1036
$$\ln(\lambda_1) = 2\ln(\chi_0 + \chi_1) + 2\ln(\chi_0 + \chi_1) + 2\ln(\chi_1 + \chi_4 + \chi_7) +$$

$$\ln(\chi_1) + \ln(\chi_1 + \chi_4 + \chi_7) + \ln(\chi_0 + \chi_1 + \chi_2 + \chi_3 + \chi_4) - \ln(\chi_1)$$
 (B32)

1037
$$\ln(\lambda_2) = 2\ln(\chi_2 + \chi_3) + 2\ln(\chi_2 + \chi_3) + 2\ln(\chi_0 + \chi_2 + \chi_5 + \chi_6) +$$

$$\ln(\chi_2) + \ln(\chi_2) + \ln(\chi_0 + \chi_1 + \chi_2 + \chi_3 + \chi_4) - \ln(\chi_2)$$
 (B33)

1038
$$\ln(\lambda_3) = 2\ln(\chi_2 + \chi_3) + 2\ln(\chi_2 + \chi_3) + 2\ln(\chi_3) +$$

$$\ln(\chi_3) + \ln(\chi_3) + \ln(\chi_0 + \chi_1 + \chi_2 + \chi_3 + \chi_4) - \ln(\chi_3)$$
 (B34)

1039
$$\ln(\lambda_4) = 2\ln(\chi_4) + 2\ln(\chi_4) + 2\ln(\chi_1 + \chi_4 + \chi_7) +$$

$$\ln(\chi_4) + \ln(\chi_1 + \chi_4 + \chi_7) + \ln(\chi_0 + \chi_1 + \chi_2 + \chi_3 + \chi_4) - \ln(\chi_4)$$
 (B35)

1040
$$\ln(\lambda_5) = 2\ln(\chi_5) + 2\ln(\chi_5) + 2\ln(\chi_0 + \chi_2 + \chi_5 + \chi_6) +$$

$$\ln(\chi_0 + \chi_5 + \chi_6) + \ln(\chi_0 + \chi_5 + \chi_6) + \ln(\chi_5 + \chi_6 + \chi_7) - \ln(\chi_5)$$
 (B36)

1041
$$\ln(\lambda_6) = 2\ln(\chi_6 + \chi_7) + 2\ln(\chi_6 + \chi_7) + 2\ln(\chi_0 + \chi_2 + \chi_5 + \chi_6) +$$

$$\ln(\chi_0 + \chi_5 + \chi_6) + \ln(\chi_0 + \chi_5 + \chi_6) + \ln(\chi_5 + \chi_6 + \chi_7) - \ln(\chi_6)$$
 (B37)

1042
$$\ln(\lambda_7) = 2\ln(\chi_6 + \chi_7) + 2\ln(\chi_6 + \chi_7) + 2\ln(\chi_1 + \chi_4 + \chi_7) +$$

$$\ln(\chi_7) + \ln(\chi_1 + \chi_4 + \chi_7) + \ln(\chi_5 + \chi_6 + \chi_7) - \ln(\chi_7)$$
 (B38)

1043

1044 **Appendix C. Thermodynamic properties of the constituent phases and**
 1045 **the relevant phases for thermodynamic modelling in this work**

1046

1047 The solid constituents used in the additivity method and eq.(23), to estimate the standard absolute
 1048 isobaric heat capacity and absolute entropy at standard state of the C-(N-)A-S-H end-members, are
 1049 shown in Table C1. The gases, aqueous species and solid phases used in the thermodynamic
 1050 modelling simulations are shown in Tables C2-C4.

1051

1052 Table C1. Thermodynamic properties of the solid constituents used to estimate Cp^o and S^o for the C-
 1053 (N-)A-S-H end-members. The reference state is 298.15 K and 1 bar.

Phase	V^o (cm ³ /mol)	$\Delta_f H^o$ (kJ/mol)	$\Delta_f G^o$ (kJ/mol)	S^o (J/mol.K)	Cp^o (J/mol.K)	Reference
Portlandite, Ca(OH) ₂	33.1	-984.7	-897.0	83.4	87.5	[93]
Amorphous SiO ₂	29.0	-903.3	-848.9	41.3	44.5	[17, 94]
Gibbsite, Al(OH) ₃	32.0	-1289	-1151	70.1	93.1	[94]
NaOH _(s)	18.8	-425.8	-379.6	64.4	59.5	[93, 95]
T2C, (CaO) _{1.5} (SiO ₂) ₁ (H ₂ O) _{2.5}	80.6	-2722	-2467	167	237	[25]

1054

1055

1056 **Table C2.** Thermodynamic properties of the gases used in the thermodynamic modelling simulations.
 1057 The reference state is 298.15 K and 1 bar.

Gas	V^o (cm ³ /mol)	$\Delta_f H^o$ (kJ/mol)	$\Delta_f G^o$ (kJ/mol.K)	S^o (J/mol.K)	Cp^o (J/mol.K)	Reference
N ₂	24790	0	0	191.6	29.1	[96]
O ₂	24790	0	0	205.1	29.3	[96]
H ₂	24790	0	0	130.7	28.8	[96]

1058

1059

1060

1061

1062

1063

1064

1065 **Table C3.** Thermodynamic properties of the aqueous species used in the thermodynamic modelling
 1066 simulations. The reference state is unit activity in a hypothetical one molal solution referenced to
 1067 infinite dilution at any temperature and pressure for aqueous species [70].

Species	V° (cm ³ /mol)	$\Delta_f H^\circ$ (kJ/mol)	$\Delta_f G^\circ$ (kJ/mol.K)	S° (J/mol.K)	C_p° (J/mol.K)	Reference
Al ³⁺	-45.2	-530.6	-483.7	-325.1	-128.7	[97]
AlO ⁺ (+ H ₂ O = Al(OH) ₂ ⁺)	0.3	-713.6	-660.4	-113	-125.1	[97]
AlO ₂ ⁻ (+ 2H ₂ O = Al(OH) ₄ ⁻)	9.5	-925.6	-827.5	-30.2	-49	[97]
AlOOH ⁰ (+ 2H ₂ O = Al(OH) ₃ ⁰)	13	-947.1	-864.3	20.9	-209.2	[97]
AlOH ²⁺	-2.7	-767.3	-692.6	-184.9	56	[97]
AlHSiO ₃ ²⁺ (+ H ₂ O = AlSiO(OH) ₃ ²⁺)	-40.7	-1718	-1541	-304.2	-215.9	[64]
AlSiO ₄ ⁻ (+ 3H ₂ O = AlSiO(OH) ₆ ⁻)	25.5	-1834	-1681	11.1	-4.6	[64]
AlSO ₄ ⁺	-6.0	-1423	-1250	-172.4	-204.0	[64]
Al(SO ₄) ₂ ⁻	31.1	-2338	-2006	-135.5	-268.4	[64]
Ca ²⁺	-18.4	-543.1	-552.8	-56.5	-30.9	[97]
CaOH ⁺	5.8	-751.6	-717	28	6	[97]
Ca(HSiO ₃) ⁺ (+ H ₂ O = CaSiO(OH) ₃ ⁺)	-6.7	-1687	-1574	-8.3	137.8	[98]
CaSiO ₃ ⁰ (+ H ₂ O = CaSiO ₂ (OH) ₂ ⁰)	15.7	-1668	-1518	-136.7	88.9	[64]
CaSO ₄ ⁰	4.7	-1448	-1310	20.9	-104.6	[98]
K ⁺	9.0	-252.1	-282.5	101	8.4	[97]
KOH ⁰	15	-474.1	-437.1	108.4	-85	[97]
KSO ₄ ⁻	27.5	-1159	-1032	146.4	-45.1	[98]
Na ⁺	-1.2	-240.3	-261.9	58.4	38.1	[97]
NaOH ⁰	3.5	-470.1	-418.1	44.8	-13.4	[97]
NaSO ₄ ⁻	18.6	-1147	-1010	101.8	-30.1	[64]
HSiO ₃ ⁻ (+ H ₂ O = SiO(OH) ₃ ⁻)	4.5	-1145	-1014	20.9	-87.2	[98]
SiO ₂ ⁰	16.1	-887.9	-833.4	41.3	44.5	[17, 99]
SiO ₃ ²⁻ (+ H ₂ O = SiO ₂ (OH) ₂ ²⁻)	34.1	-1099	-938.5	-80.2	119.8	[64]
S ₂ O ₃ ²⁻	27.6	-649.9	-520.0	66.9	-238.5	[97]
HSO ₃ ⁻	33.0	-627.7	-529.1	139.7	-5.4	[97]
SO ₃ ²⁻	-4.1	-636.9	-487.9	-29.3	-281.0	[97]
HSO ₄ ⁻	34.8	-889.2	-755.8	125.5	22.7	[97]
SO ₄ ²⁻	12.9	-909.7	-744.5	18.8	-266.1	[97]
H ₂ S ⁰	35.0	-39.0	-27.9	125.5	179.2	[99]
HS ⁻	20.2	-16.2	12.0	68.2	-93.9	[97]
S ²⁻	20.2	92.2	120.4	68.2	-93.9	[63]
Mg ²⁺	-22.0	-465.9	-454.0	-138.1	-21.7	[97]
MgOH ⁺	1.6	-690.0	-625.9	-79.9	129.2	[97]
MgHSiO ₃ ⁺ (+ H ₂ O = MgSiO(OH) ₃ ⁺)	-10.9	-1614	-1477	-99.5	158.6	[97]
MgSO ₄ ⁰	1.8	-1369	-1212	-50.9	-90.3	[63, 97]
MgSiO ₃ ⁰ (+ H ₂ O = MgSiO ₂ (OH) ₂ ⁰)	12.1	-1597	-1425	-218.3	98.2	[63]
OH ⁻	-4.7	-230	-157.3	-10.7	-136.3	[97]
H ⁺	0	0	0	0	0	[97]
H ₂ O ⁰	18.1	-285.9	-237.2	69.9	75.4	[100]
N ₂ ⁰	33.4	-10.4	18.2	95.8	234.2	[99]
O ₂ ⁰	30.5	-12.2	16.4	109	234.1	[99]

1068

1069

1070

1071

1072 **Table C4.** Thermodynamic properties of the solid phases used in the thermodynamic modelling
1073 simulations. The reference state is 298.15 K and 1 bar.

Phase	V^* (cm ³ /mol)	$\Delta_f H^*$ (kJ/mol)	$\Delta_f G^*$ (kJ/mol.K)	S^* (J/mol.K)	C_p^* (J/mol.K)	Reference
Al(OH) ₃ (microcrystalline)	32.0	-1265	-1148	140	93.1	[101]
Portlandite, Ca(OH) ₂	33.1	-984.7	-897	83.4	87.5	[93]
Amorphous SiO ₂	29.0	-903.3	-849	41.3	44.5	[17, 94]
C ₂ AH ₈	90.1	-5278	-4696	450	521	[101]
C ₃ AH ₆	150	-5537	-5008	422	446	[101]
C ₄ AH ₁₃	27.4	-8302	-7327	700	930	[66]
C ₄ AH ₁₉	382	-1002	-8750	1120	1382	[101]
C ₄ AH ₁₀	194	-5388	-4623	610	668	[101]
Monosulfate, C ₄ AsH ₁₂	309	-8750	-7779	821	942	[64]
Stratlingite, C ₂ ASH ₈	21.6	-6360	-5705	546	603	[64]
Ettringite, C ₆ As ₃ H ₃₂	707	-17535	-15206	1900	2174	[66]
Hydrotalcite, M ₄ AH ₁₀	220	-7196	-6395	549	649	[66]
Brucite, Mg(OH) ₂	24.6	-923	-832	63.1	77.3	[94]
The 'downscaled CSH3T' model ^a						
TobH, (CaO) ₁ (SiO ₂) _{1.5} (H ₂ O) _{2.5}	85.0	-2833	-2562	153	231	[25]
T5C, (CaO) _{1.25} (SiO ₂) _{1.25} (H ₂ O) _{2.5}	79.3	-2782	-2519	160	234	[25]
T2C, (CaO) _{1.5} (SiO ₂) ₁ (H ₂ O) _{2.5}	80.6	-2722	-2467	167	237	[25]

1074 ^a The mixing rules used to describe the downscaled CSH3T model and the thermodynamic properties
1075 that define the TobH, T5C and T2C end-members in GEM-Selektor are the same as those described
1076 in [25] for this model. The Gibbs free energies (and thus the enthalpies) of these components are
1077 modified slightly to the corresponding values used to define the TobH*, T5C* and T2C* end-
1078 members of the CNASH_ss model (Table 2).

1079

1080

1081

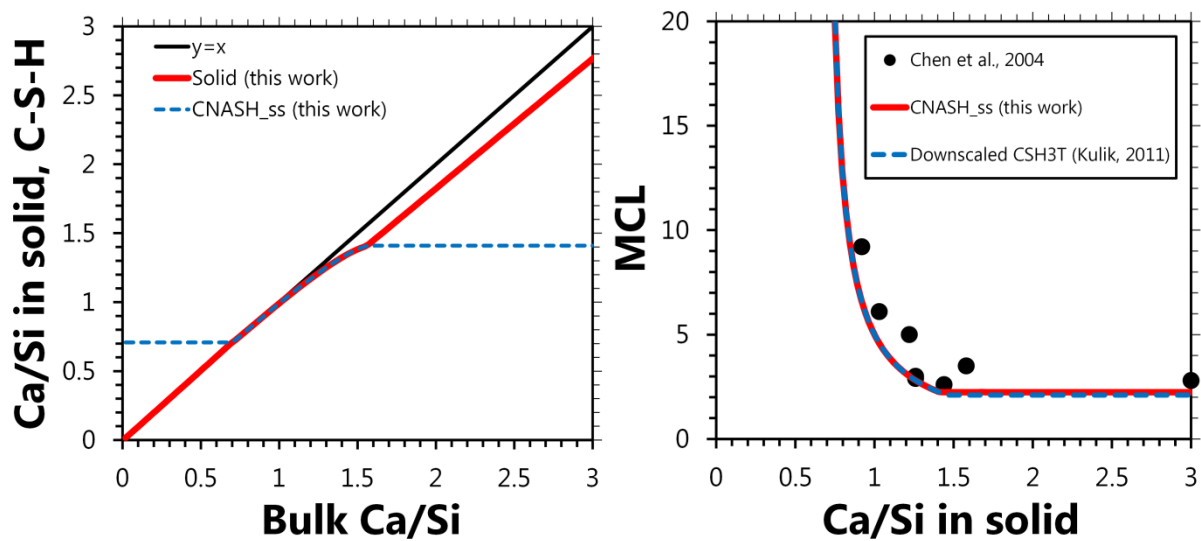
1082 **Appendix D. Additional simulation results used to validate the**
1083 **thermodynamic model**

1084

1085 Additional simulation results that were used to validate the thermodynamic model are shown in

1086 Figures D1-D6.

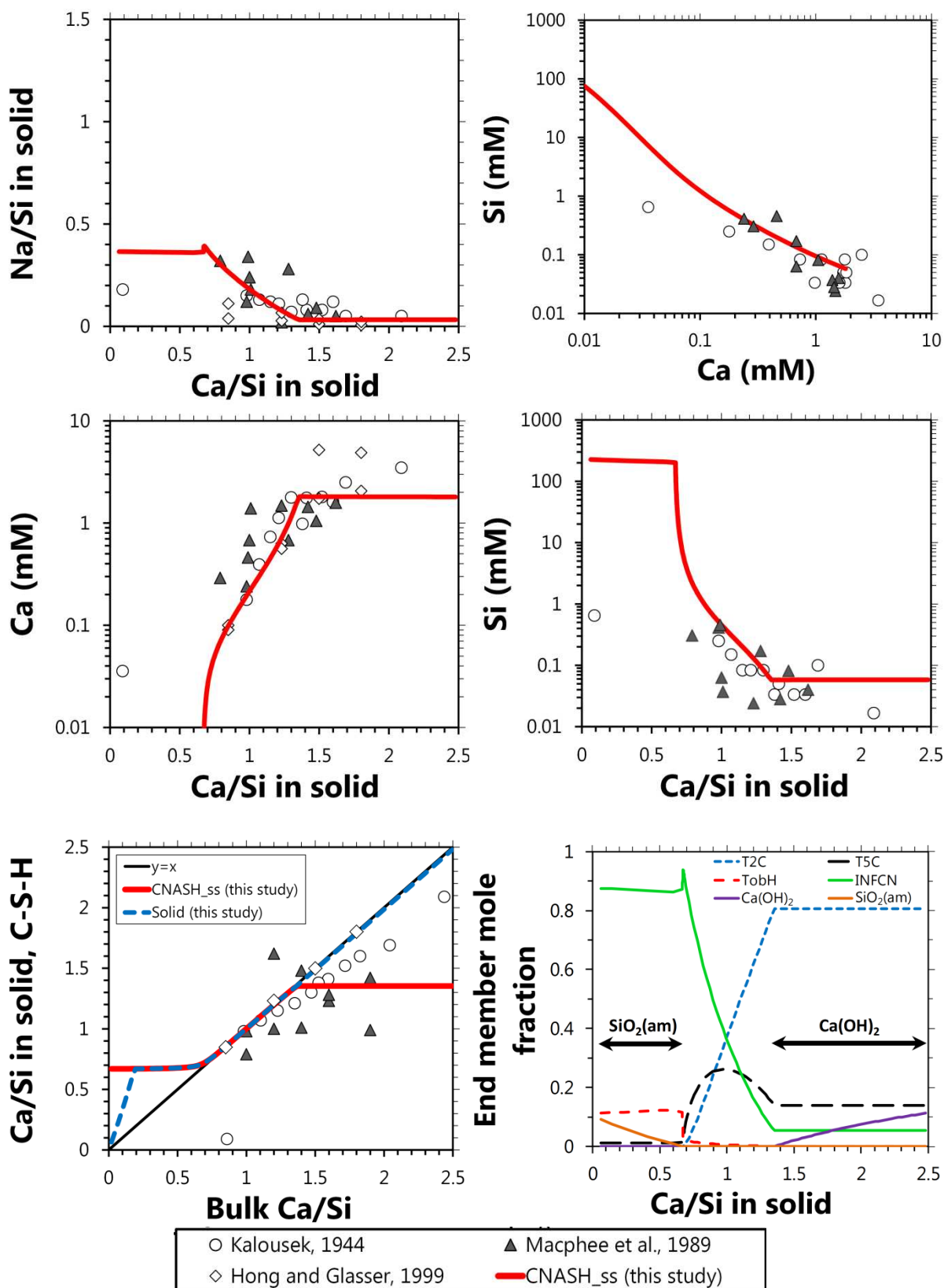
1087



1088

1089 **Figure D1.** Simulation results (25°C, 1 bar, 0.25 M NaOH/solids mass ratio = 50) using the
1090 thermodynamic model developed here (CNASH_ss) in addition to those presented in Figure 2. The
1091 MCL calculations are compared to the data reported in [8] and the simulation results using the
1092 downscaled CSH3T model [25]. The thermodynamic properties of the phases included in these
1093 simulations are given in Appendix C.

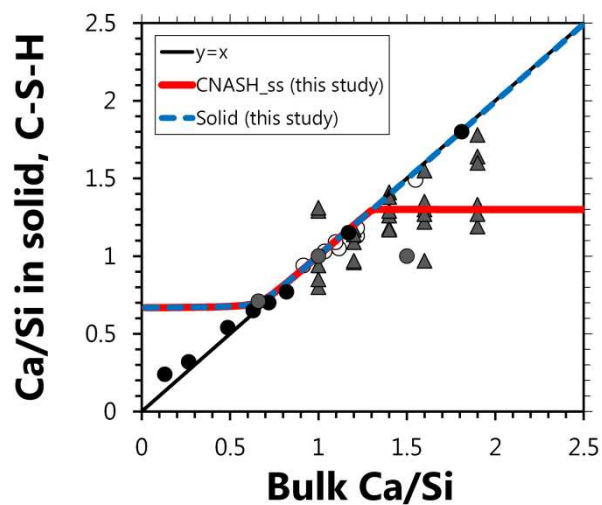
1094



1099 **Figure D2.** Comparison of the simulation results (25°C, 1 bar, 0.25 M NaOH/solids mass ratio = 50)
 1100 using the thermodynamic model developed here (CNASH_ss, bold red traces) to published solubility
 1101 data in the CaO-Na₂O-SiO₂-H₂O system at alkali concentrations 0.1 M ≤ [NaOH] ≤ 0.3 M [76, 80, 81].
 1102 The thermodynamic properties of the phases included in these simulations are given in Appendix C.

1103

1104



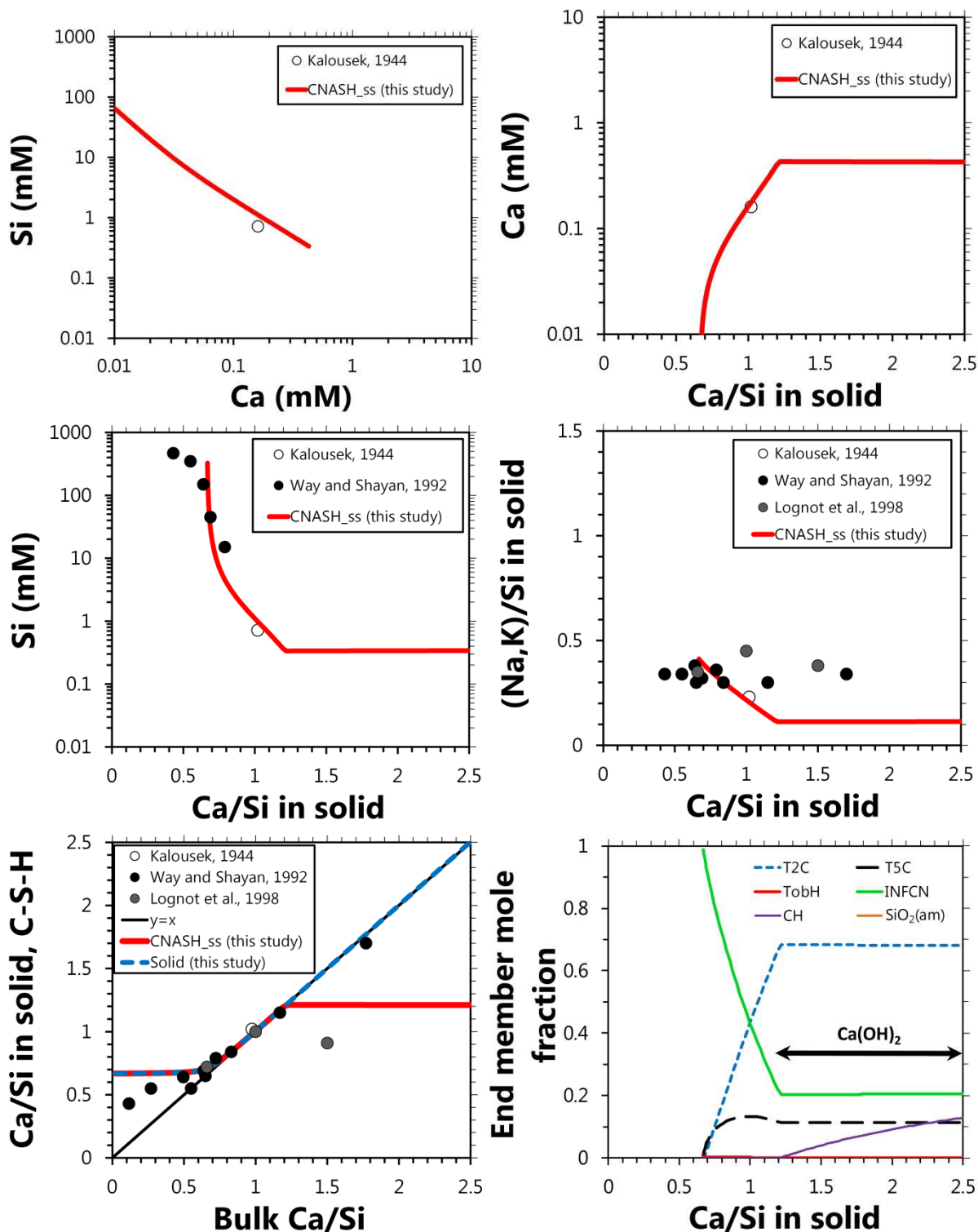
1105



1106

1107 **Figure D3.** Comparison of the simulation results (25°C, 1 bar, 0.5 M NaOH/solids mass ratio = 50)
1108 using the thermodynamic model developed here (CNASH_ss, bold red traces) to solid chemistry data
1109 in the CaO-Na₂O-SiO₂-H₂O system at alkali concentrations 0.3 M ≤ [NaOH] ≤ 0.8 M [76, 80, 81], in
1110 addition to the results shown in Figure 3 for this system. The thermodynamic properties of the
1111 phases included in these simulations are given in Appendix C.
1112

1113



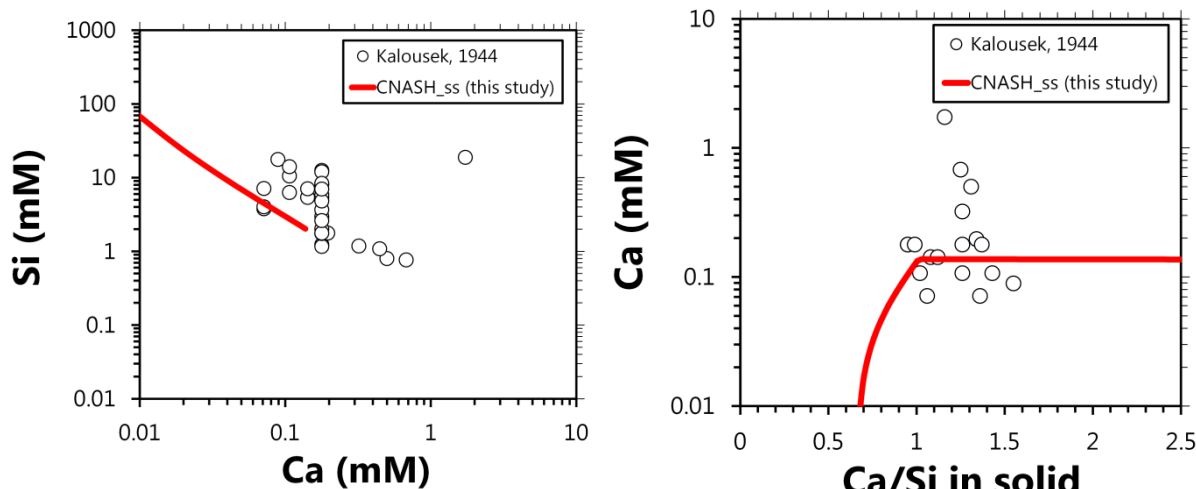
1114

1115

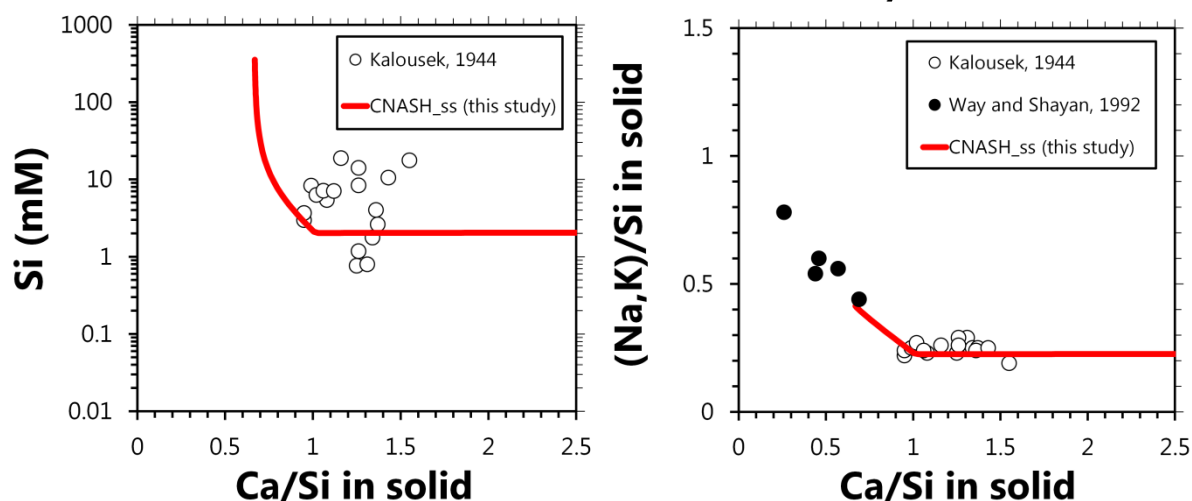
1116

1117 **Figure D4.** Comparison of the simulation results (25°C, 1 bar, 1 M NaOH/solids mass ratio = 50) using
 1118 the thermodynamic model developed here (CNASH_{ss}, bold red traces) to solubility and solid phase
 1119 chemistry data in the CaO-Na₂O-SiO₂-H₂O system at alkali concentrations 0.8 M ≤ [NaOH] ≤ 1 M [75,
 1120 77, 80]. The corresponding end member mole fraction results are also shown. The thermodynamic
 1121 properties of the phases included in these simulations are given in Appendix C.
 1122

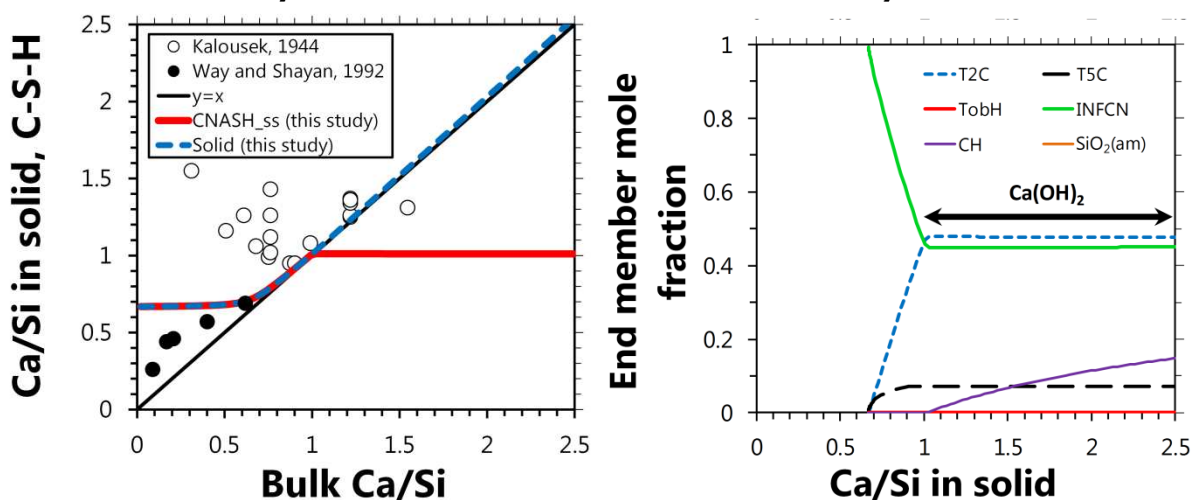
1123



1124



1125

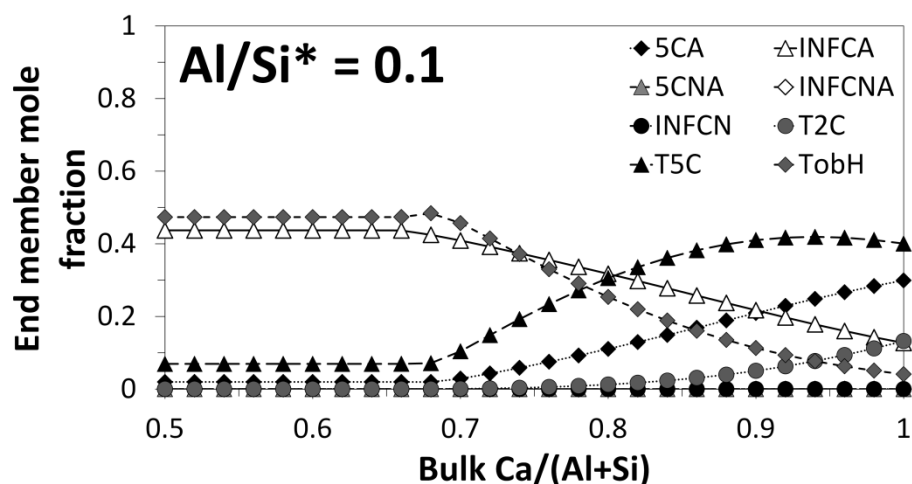


1126

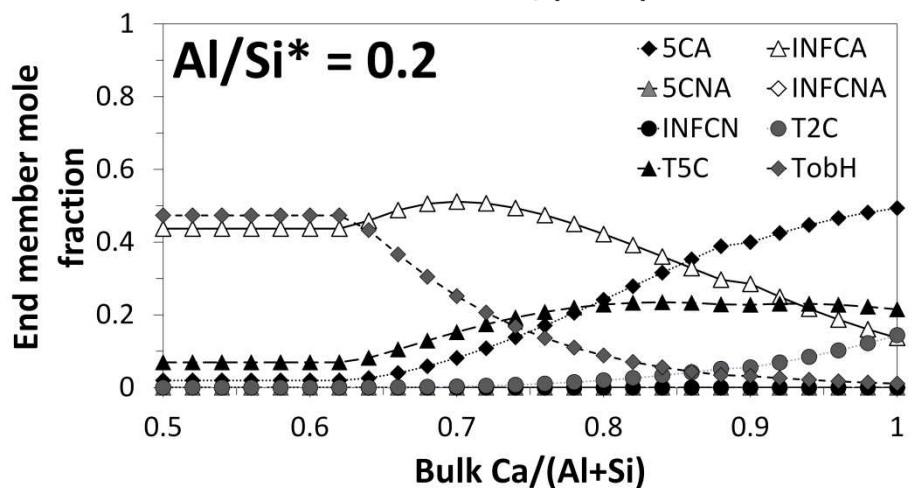
1127 **Figure D5.** Comparison of the simulation results (25°C, 1 bar, 3 M NaOH/solids mass ratio = 50) using
 1128 the thermodynamic model developed here (CNASH_{ss}, bold red traces) to solubility and solid phase
 1129 chemistry data in the CaO-Na₂O-SiO₂-H₂O system at alkali concentrations 1 M ≤ [NaOH] ≤ 5 M [77,
 1130 80]. The corresponding end member mole fraction results are also shown. The thermodynamic
 1131 properties of the phases included in these simulations are given in Appendix C.

1132

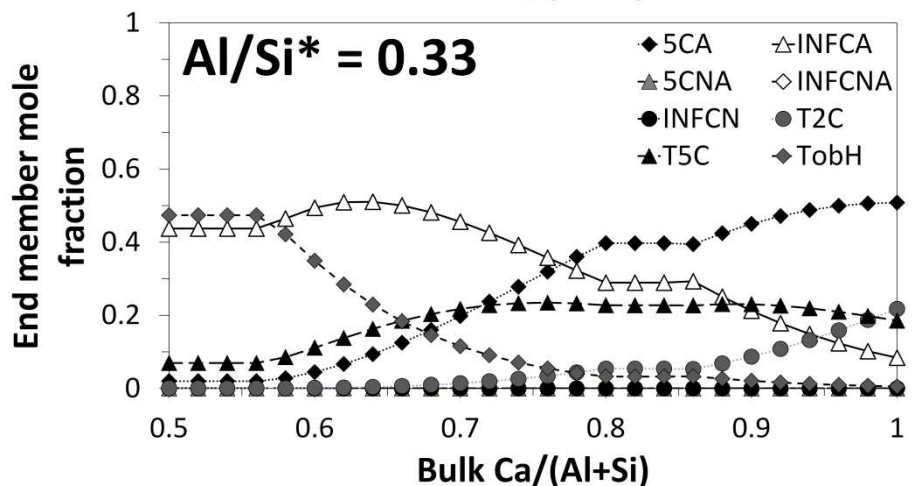
1133



1134



1135



1136

1137 **Figure D6.** End member mole fractions corresponding to the simulation results shown in Figure 5

1138 (25°C, 1 bar, water/solids mass ratio = 50). Al/Si^* = bulk Al/Si . The thermodynamic properties of the

1139 phases included in these simulations are given in Appendix C.

1140

1141 **Appendix E. Additional details of the AAS cements simulated by**
 1142 **thermodynamic modelling**

1143

1144 The slag reaction extents, curing times and activating conditions used to simulate the pore solution
 1145 chemistry of AAS cements (Figure 6) are shown in Table E1.

1146

1147 **Table E1.** Slag reaction extents, curing times and activating conditions used to simulate the pore
 1148 solution chemistry of AAS cements.

System (corresponding to the legend labels in Figure 6)	Curing time (days)	Activator	Water/binder	Slag reaction extent used in simulations (%)	Reference
Gruskovnjak et al., 2006	1	Na ₂ SiO ₃ ·5H ₂ O	0.3 ^a	32	[71]
Gruskovnjak et al., 2006	7	Na ₂ SiO ₃ ·5H ₂ O	0.3 ^a	36	[71, 87]
Gruskovnjak et al., 2006	28	Na ₂ SiO ₃ ·5H ₂ O	0.3 ^a	38	[71, 87]
Gruskovnjak et al., 2006	180	Na ₂ SiO ₃ ·5H ₂ O	0.3 ^a	42	[71, 87]
Puertas et al., 2004	7	Na ₂ O·1.5SiO ₂ ·xH ₂ O	0.5 ^b	36	[82]
Puertas et al., 2004	7	NaOH	0.5 ^b	36	[82]
Lloyd et al., 2010	90	Na ₂ O·mSiO ₂ ·xH ₂ O	0.35	40	[83]
Song and Jennings, 1999	28	1 M NaOH	0.45 ^c	36	[84]
Song and Jennings, 1999	28	0.5 M NaOH	0.45 ^c	31	[84]
Song and Jennings, 1999	28	0.1 M NaOH	0.45 ^c	26	[84]
Song and Jennings, 1999	41	H ₂ O	0.45 ^c	21	[84]
Song and Jennings, 1999	44	1 M NaOH	0.45 ^c	39	[84]
Song and Jennings, 1999	44	0.5 M NaOH	0.45 ^c	34	[84]
Song and Jennings, 1999	44	0.1 M NaOH	0.45 ^c	29	[84]

1149 ^a water/cement.

1150 ^b (water + activator)/slag.

1151 ^c liquid/slag.

1152

1153

1154